



FEASIBILITY OF IDENTIFYING NON-LINEAR VIBRATORY SYSTEMS CONSISTING OF UNKNOWN POLYNOMIAL FORMS

C. M. RICHARDS AND R. SINGH

*Acoustics and Dynamics Laboratory, Department of Mechanical Engineering,
The Ohio State University, Columbus, OH 43210-1107, U.S.A.*

(Received 23 March 1998, and in final form 14 August 1998)

System identification techniques for non-linear systems may require *a priori* knowledge of the nature and mathematical form of the non-linearities. However, for practical systems, this is not always possible. As a result, non-linearities are often approximated and questions remain as to whether a reasonably accurate model can be determined. Concurrently, under experimental conditions, some means of quantifying the amount of measurement noise present in the identification process must also be obtained. To resolve such issues, a discrete non-linear system problem is formulated in the presence of uncorrelated noise and critically examined from the standpoint of identification. Coherence functions are introduced which are based on a “reverse path” spectral approach recently developed by the authors for multi-degree-of-freedom systems. These coherence functions, as calculated from conditioned spectra, indicate the extent of uncorrelated noise present and the accuracy of assumed mathematical models employed for describing non-linear systems. Using several example simulation systems, including a system with a continuous non-linearity described by a non-integer exponent, both temporal and spectral identification techniques are employed to study the issues described above.

© 1999 Academic Press

1. INTRODUCTION

Consider a non-linear structural or mechanical system described by the following set of N coupled differential equations:

$$\mathbf{M}\ddot{\mathbf{x}}(t) + \mathbf{d}(\mathbf{x}(t), \dot{\mathbf{x}}(t)) = \mathbf{f}(t), \quad (1)$$

where \mathbf{M} is the time-invariant mass matrix, $\mathbf{x}(t)$ and $\mathbf{f}(t)$ are the generalized displacement and force vectors, and $\mathbf{d}(\mathbf{x}(t), \dot{\mathbf{x}}(t))$ is a vector of motion dependent

restoring force functions. Decompose $\mathbf{d}(\mathbf{x}(t), \dot{\mathbf{x}}(t))$ as follows:

$$\mathbf{d}(\mathbf{x}(t), \dot{\mathbf{x}}(t)) = \mathbf{C}\dot{\mathbf{x}}(t) + \mathbf{K}\mathbf{x}(t) + \mathbf{d}_n(\mathbf{x}(t), \dot{\mathbf{x}}(t)), \quad (2a)$$

$$\mathbf{M}\ddot{\mathbf{x}}(t) + \mathbf{C}\dot{\mathbf{x}}(t) + \mathbf{K}\mathbf{x}(t) + \mathbf{d}_n(\mathbf{x}(t), \dot{\mathbf{x}}(t)) = \mathbf{f}(t), \quad (2b)$$

where \mathbf{C} and \mathbf{K} are the time-invariant linear damping and linear stiffness matrices, and $\mathbf{d}_n(\mathbf{x}(t), \dot{\mathbf{x}}(t))$ is a vector consisting of only non-linear terms. When the system is linear, i.e., $\mathbf{d}_n(\mathbf{x}(t), \dot{\mathbf{x}}(t)) = \{0\}$, or linearized to yield effective damping \mathbf{C}_e and stiffness \mathbf{K}_e matrices, identification methods can estimate parameters from measured time or frequency domain data in the form of natural frequencies ω_r , mode shapes ϕ_r and damping ratios ζ_r [1]. However, complexities such as high modal density, heavily damped modes and measurement noise complicate the accurate determination of these parameters. These complications may be alleviated using mode indicator functions to determine valid modes [1] and proper frequency response estimators, such as “ H_1 ” or “ H_2 ”, to minimize uncorrelated measurement noise [2, 3]. Nonetheless, it is difficult to construct \mathbf{M} , \mathbf{C} and \mathbf{K} unless a computational model is available.

To worsen the problem of identification, the effects of $\mathbf{d}_n(\mathbf{x}(t), \dot{\mathbf{x}}(t))$ for many physical non-linear systems may substantially influence the dynamic response $\mathbf{x}(t)$ [4–6]. Consequently, modal testing and similar methods are no longer valid. Under these circumstances identification methods for non-linear systems must be employed. Unfortunately, literature on such techniques is rather sparse as discussed in reference [7]. A temporal method known as the Restoring Force or Force State Mapping Method has been developed [8, 9] and investigated [10, 11]. Likewise, a spectral method based upon a “reverse path” analysis has been formulated for single-degree-of-freedom systems [12–15] and recently modified for multi-degree-of-freedom systems [7]. However, many issues remain unresolved before such methods can be applied to practical problems. Three key questions follow: (1) Should there be an *a priori* knowledge of the nature and mathematical form of $\mathbf{d}_n(\mathbf{x}(t), \dot{\mathbf{x}}(t))$ before the identification process is initiated? If not, will an appropriate model result from the approximation of $\mathbf{d}_n(\mathbf{x}(t), \dot{\mathbf{x}}(t))$? (2) Is the identification problem compounded by the presence of measurement noise? (3) Can coherence techniques be used to facilitate the identification process? These issues are addressed in this article *via* several simulation examples. Only continuous non-linearities will be considered with emphasis on polynomial forms. The “Reverse Path” Spectral Method for multi-degree-of-freedom systems [7] will be the chief method of evaluation. However, the Temporal Method [8–11] will also be utilized for one example to illustrate whether the issues raised here are method dependent. The effects of measurement noise on the estimates are examined for moderate and high levels of uncorrelated noise. Also, the performance of the Spectral Method and the associated coherence functions will be critically assessed under conditions that the nature or shape of the non-linearities is unknown but approximated by alternative mathematical functions.

2. PROBLEM FORMULATION

2.1. SCOPE

Consider the two-degree-of-freedom system of Figure 1(a) consisting of only one non-linear spring element with elastic force $f_{12}^e(t)$. Therefore define $\mathbf{d}_n(\mathbf{x}(t), \dot{\mathbf{x}}(t)) = \mathbf{d}_n(\mathbf{x}(t))$ and equation (2b) becomes

$$\mathbf{M}\ddot{\mathbf{x}}(t) + \mathbf{C}\dot{\mathbf{x}}(t) + \mathbf{K}\mathbf{x}(t) + \mathbf{d}_n(\mathbf{x}(t)) = \mathbf{f}(t). \tag{3}$$

Masses, linear damping and linear stiffness coefficients are listed in Table 1 along with the system's modal properties determined by assuming that $\mathbf{d}_n(\mathbf{x}(t)) = \{0\}$. Refer to Appendix A for a list of symbols. Also, refer to prior work by Richards and Singh [7] for the identification of 3- and 5-degree-of-freedom systems. Several

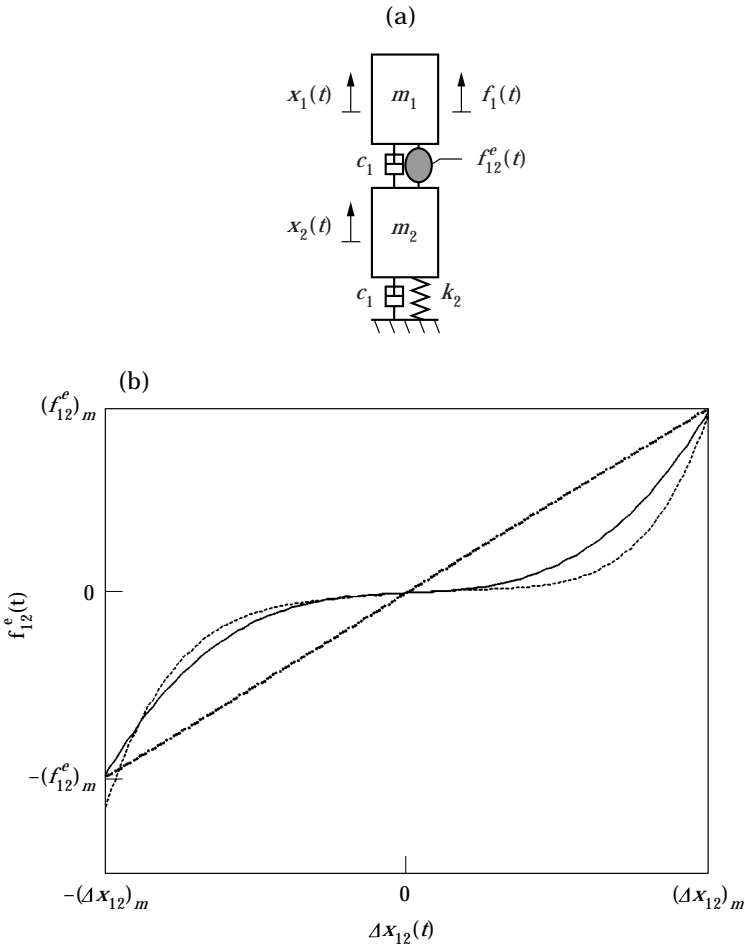


Figure 1. Simulation examples. (a) Two-degree-of-freedom system with a non-linear spring element of elastic force $f_{12}^e(t)$. (b) Plots of non-linear elastic forces. —, $f_{12}^e(t)$ of Example I; ---, $f_{12}^e(t)$ of Example II; ···, linear component of $f_{12}^e(t)$, i.e., $k_1 \Delta x_{12}(t)$.

TABLE 1

True linear system properties of Examples I, II and IV given $\mathbf{d}_n(\mathbf{x}(t)) = \{0\}$

	DOF, i	m_i (kg)	c_i (N · s/m)	k_i (kN/m)
Physical properties	1	1·0	10·0	100·0
	2	1·0	10·0	100·0
	Mode, r	ω_r (Hz)	ζ_r (%)	ϕ_r
Modal properties	1	31·1	1·0	{1·0, 0·6}
	2	81·4	2·6	{-0·6, 1·0}

In Example III $c_i = 100$ Ns/m, other physical properties remain the same.

examples will be examined here where the non-linear spring stiffness is described by different mathematical forms. Examples I and II are discussed first where the elastic force $f_{12}^e(t)$ of Example I is described by linear and cubic terms and $f_{12}^e(t)$ of Example II is described by linear, quadratic and 5th order terms, as listed in Table 2. Therefore,

$$\text{Example I: } \mathbf{d}_n(\mathbf{x}(t)) = \begin{bmatrix} \beta_3 \Delta x_{12}(t)^3 \\ -\beta_3 \Delta x_{12}(t)^3 \end{bmatrix},$$

$$\text{Example II: } \mathbf{d}_n(\mathbf{x}(t)) = \begin{bmatrix} \beta_2 \Delta x_{12}(t)^2 + \beta_5 \Delta x_{12}(t)^5 \\ -\beta_2 \Delta x_{12}(t)^2 - \beta_5 \Delta x_{12}(t)^5 \end{bmatrix}, \quad (4a, b)$$

where $\Delta x_{12}(t) = x_1(t) - x_2(t)$ and β_2, β_3 and β_5 are coefficients of the polynomial terms describing $f_{12}^e(t)$. By applying a synthesized Gaussian random excitation $f_i(t)$ with $|f_i(t)| = 60$ N-rms, mean = 0 and variance = 1, $\mathbf{x}(t) = [x_1(t) \ x_2(t)]^T$, $\dot{\mathbf{x}}(t)$ and $\ddot{\mathbf{x}}(t)$ for both examples are calculated using a 5th order Runge–Kutta Fehlberg numerical integration method. The time steps (Δt) are held constant so that the Fast Fourier Transform (FFT) can be applied to the data, and high frequency numerical simulation errors are minimized by choosing a Nyquist frequency eight times greater than the highest frequency of interest. The following numerical simulation parameters are used: $\Delta t = 0\cdot5$ ms, number of samples = $15 \cdot (2^{14})$, total

TABLE 2

True non-linear elastic force $f_{12}^e(t)$ of Examples I–IV

Example	$f_{12}^e(t)$	Coefficients
I, III	$k_1 \Delta x_{12}(t) + \beta_3 \Delta x_{12}(t)^3$	$\beta_3 = 500\cdot0 \text{ MN/m}^3$
II	$k_1 \Delta x_{12}(t) + \beta_2 \Delta x_{12}(t)^2 + \beta_5 \Delta x_{12}(t)^5$	$\beta_2 = -1\cdot0 \text{ MN/m}^2, \beta_5 = 10\cdot0 \text{ GN/m}^5$
IV	$k_1 \Delta x_{12}(t) + \eta \cdot \text{sgn}(\Delta x_{12}(t)) \Delta x_{12}(t) ^{1\cdot8}$	$\eta = 1\cdot0 \text{ MN/m}^{1\cdot8}$

period = $15 \cdot (2^{13})$ ms. Corresponding stiffness curves are illustrated in Figure 1(b) where $(\Delta x_{12}(t))_m$ and $(f_{12}^e(t))_m$ are the maximum $\Delta x_{12}(t)$ and $f_{12}^e(t)$ experienced by Examples I and II in the numerical simulations.

Under experimental testing conditions, the modal properties of Table 1 are typically identified from the input/output data of Examples I and II using well accepted modal analysis or comparable system identification techniques. However, erroneous modal parameters may result, as illustrated in the frequency domain to follow. First, take the Fourier transform $F[\cdot]$ of equation (3):

$$\mathbf{B}(\omega)\mathbf{X}(\omega) + \Gamma_n(\omega) = \mathbf{F}(\omega), \quad \mathbf{X}(\omega) = F[\mathbf{x}(t)], \quad \Gamma_n(\omega) = F[\mathbf{d}_n(\mathbf{x}(t))],$$

$$\mathbf{F}(\omega) = F[\mathbf{f}(t)], \quad \mathbf{B}(\omega) = -\omega^2\mathbf{M} + i\omega\mathbf{C} + \mathbf{K}, \quad \mathbf{B}(\omega) = \mathbf{H}(\omega)^{-1} \quad (5a-f)$$

where $\mathbf{B}(\omega)$ and $\mathbf{H}(\omega)$ are the linear dynamic stiffness and compliance matrices, respectively. Contamination of $\mathbf{H}(\omega)$ results due to the presence of $\Gamma_n(\omega)$. Figure 2 illustrates a sample result in terms of $\hat{H}_{21}^{[1]}(\omega)$ that is estimated from the data of Example I by the “ H_1 ” frequency response estimator [2, 3], where $\hat{}$ signifies estimated, superscript [1] signifies an “ H_1 ” estimate, and subscripts 2 and 1 signify that $\hat{H}_{21}^{[1]}(\omega)$ is a cross-point function between $x_2(t)$ and $f_1(t)$. The following procedure is used for all spectral calculations. The sampled data are first divided into 30 averages consisting of 2^{13} samples per average. Since the Nyquist frequency is much greater than the highest frequency of interest, an eighth order Chebyshev type I low pass filter with a cut-off frequency at 100 Hz is applied next. The data are then resampled at a new $\Delta t' = 8 \cdot \Delta t$ and a Hanning window is employed to minimize leakage errors. Also shown in Figure 2 is a true linear $H_{21}(\omega)$ that is synthesized from the modal parameters of Table 1. As illustrated, the first mode of $\hat{H}_{21}^{[1]}(\omega)$ has shifted up in frequency, as expected due to the presence of the hardening spring non-linearity located between m_1 and m_2 . Worse is the effect on the second mode which is highly corrupted by the non-linearity. Frequency domain modal parameter estimation techniques would lead to erroneous results for the natural frequency of the first mode and modal parameters of the second mode would be unattainable. The same procedure is also applied to the data of Example II and problems similar to Example I are encountered. Also, comparable problems are encountered when time domain techniques [1] are used to estimate the parameters of Examples I and II. Therefore, appropriate temporal or spectral non-linear system identification methods must be employed in order to determine the true parameters of these examples. However, this initial analysis may serve as a strategy for locating non-linearities. First, observe from Table 1 that the mode shape of the second mode ϕ_2 has a larger relative displacement between m_1 and m_2 than the first mode ϕ_1 . This larger displacement amplifies the non-linear behavior of the elastic force $f_{12}^e(t)$ causing mode 2 to be more corrupted. Consequently, by studying frequency response functions at various excitation levels and examining the deformation shapes of the modes most corrupted by the non-linear response, non-linearities may be located where the relative displacements of these mode shapes are largest. For Example I lower excitation levels would be necessary which lessen the corruption of mode 2 such that a deformation shape could be obtained. It should also be noted that this strategy

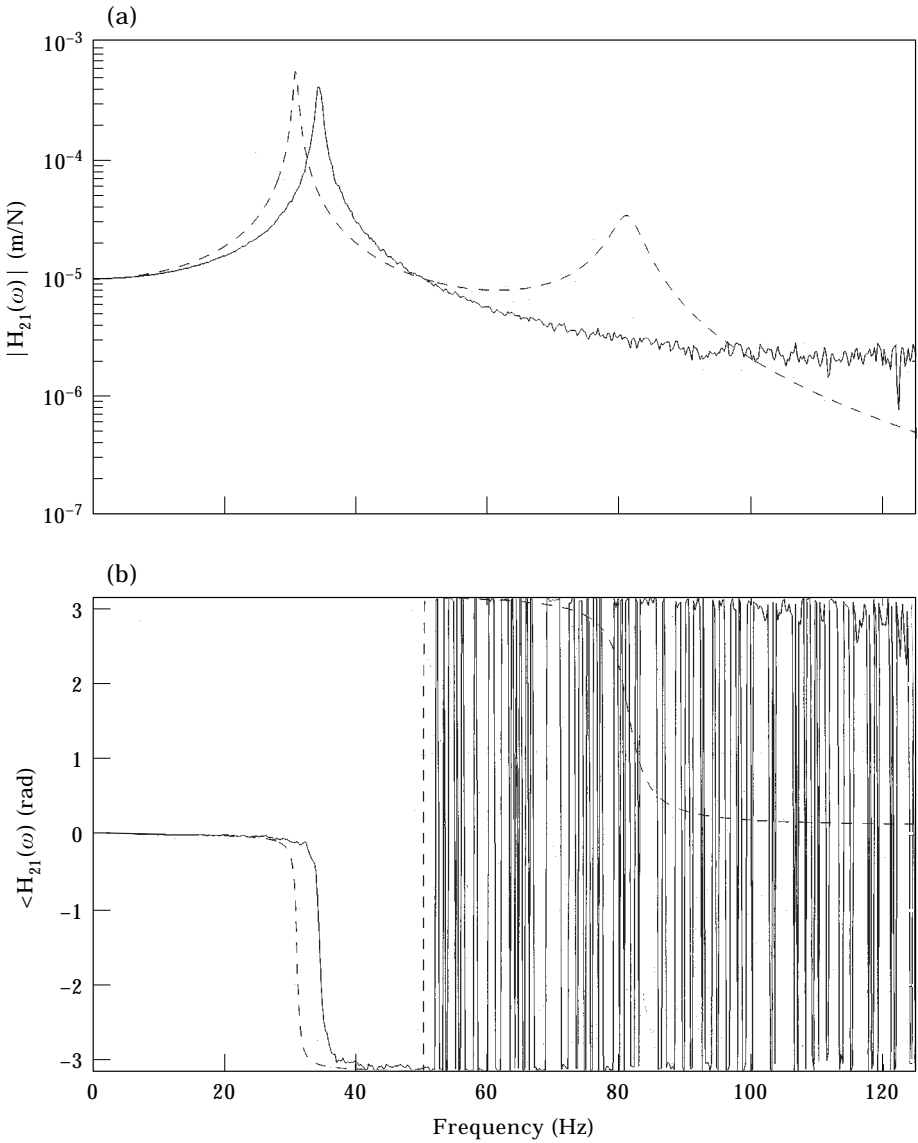


Figure 2. Dynamic compliance spectra of Example I. (a) Magnitude of $H_{21}(\omega)$. (b) Phase of $H_{21}(\omega)$. —, $\hat{H}_{21}^l(\omega)$; ---, $H_{21}(\omega)$.

will only be successful for systems with well defined deformation patterns. This issue itself warrants further studies in the presence of non-linear elements.

2.2. METHODOLOGY

The identification schemes for non-linear systems discussed in this article estimate the linear properties and non-linear elastic forces by fitting a mathematical model of the following form to the measured or simulated excitation and response data

$$\hat{\mathbf{M}}\ddot{\mathbf{x}}(t) + \hat{\mathbf{z}}(\mathbf{x}(t), \dot{\mathbf{x}}(t)) = \mathbf{f}(t), \tag{6}$$

where $\hat{\mathbf{M}}$ is the estimated mass matrix and $\hat{\mathbf{z}}(\mathbf{x}(t), \dot{\mathbf{x}}(t))$ is a vector of motion dependent functions which estimate the system's constraint forces. Considering only Examples I and II with linear viscous damping and a non-linear elastic force $f_{12}^e(t)$, write $\hat{\mathbf{z}}(\mathbf{x}(t), \dot{\mathbf{x}}(t))$ as

$$\hat{\mathbf{z}}(\mathbf{x}(t), \dot{\mathbf{x}}(t)) = \hat{\mathbf{C}}\dot{\mathbf{x}}(t) + \hat{\mathbf{K}}\mathbf{x}(t) + \hat{\mathbf{z}}_n(\mathbf{x}(t)), \quad \hat{\mathbf{z}}_n(\mathbf{x}(t)) = \sum_{j=1}^n \hat{\mathbf{a}}_j y_j(\Delta x_{12}(t)), \quad (7a, b)$$

where $\hat{\mathbf{C}}$ and $\hat{\mathbf{K}}$ are estimated linear damping and stiffness matrices and $\hat{\mathbf{z}}_n(\mathbf{x}(t))$ contains only the non-linear terms of an assumed model $p_{12}^e(t)$ for describing the true elastic force $f_{12}^e(t)$. The n unique non-linear functions $y_j(\Delta x_{12}(t))$ transform the relative displacement $\Delta x_{12}(t)$ into the form of each non-linear term of $p_{12}^e(t)$ and $\hat{\mathbf{a}}_j$ are coefficient vectors containing estimates of the coefficients of the non-linear terms, i.e., $\hat{\mathbf{a}}_j = [\hat{a}_j - \hat{a}_j]^T$. Therefore, equation (6) becomes

$$\hat{\mathbf{M}}\ddot{\mathbf{x}}(t) + \hat{\mathbf{C}}\dot{\mathbf{x}}(t) + \hat{\mathbf{K}}\mathbf{x}(t) + \sum_{j=1}^n \hat{\mathbf{a}}_j y_j(\Delta x_{12}(t)) = \mathbf{f}(t). \quad (8)$$

The Restoring Force Method is a temporal method which estimates the masses, linear damping and linear stiffness coefficients as well as the coefficients of the non-linear elastic force terms by fitting the model (8) to the measured or simulated excitation and response data in the time domain [11, 12]. The system of equations (8) is not fit to the data simultaneously; rather, the method begins with the non-homogeneous equation describing the motion of the forced degree of freedom (m_1) and then iterates to the equation describing the motion of the adjacent degree of freedom (m_2). Alternatively, the Multi-Degree-of-Freedom ‘‘Reverse Path’’ Spectral Method, referred to as the Spectral Method from this point forth, is a frequency domain system identification approach proposed by us in a recent article [7]. Applying the Fourier transform $\mathbf{F}[\cdot]$ to equation (8):

$$\begin{aligned} \hat{\mathbf{B}}(\omega)\mathbf{X}(\omega) + \sum_{j=1}^n \hat{\mathbf{a}}_j Y_j(\omega) &= \mathbf{F}(\omega), & \mathbf{X}(\omega) &= \mathbf{F}[\mathbf{x}(t)], & Y_j(\omega) &= \mathbf{F}[y_j(\Delta x_{12}(t))], \\ \mathbf{F}(\omega) &= \mathbf{F}[\mathbf{f}(t)], & \hat{\mathbf{B}}(\omega) &= -\omega^2 \hat{\mathbf{M}} + i\omega \hat{\mathbf{C}} + \hat{\mathbf{K}} \end{aligned} \quad (9a-e)$$

where $\hat{\mathbf{B}}(\omega)$ is an estimate of $\mathbf{B}(\omega)$. For the ‘‘reverse path’’ analysis, the excitation $\mathbf{F}(\omega)$ is treated as an output to the model and the total response $\mathbf{X}(\omega)$ along with the non-linear functions $Y_j(\omega)$ are treated as inputs to the model [7]. Therefore, rewrite equation (9a) as

$$\mathbf{F}(\omega) = \hat{\mathbf{B}}(\omega)\mathbf{X}(\omega) + \sum_{j=1}^n \hat{\mathbf{a}}_j Y_j(\omega). \quad (10)$$

Equation (10) is also shown graphically in Figure 3(a). By applying spectral conditioning techniques [7, 16], Figure 3(a) can be redrawn as a conditioned model with uncorrelated inputs as shown in Figure 3(b), where $Y_{j(-1;j-1)}(\omega)$ are

conditioned spectra of the non-linear functions $Y_j(\omega)$, and $\mathbf{X}_{(-1:n)}(\omega)$ contains only the linear spectral components of the total response $\mathbf{X}(\omega)$. Therefore, the linear path $\hat{\mathbf{B}}(\omega)$ can now be estimated without any influence from the non-linearities.

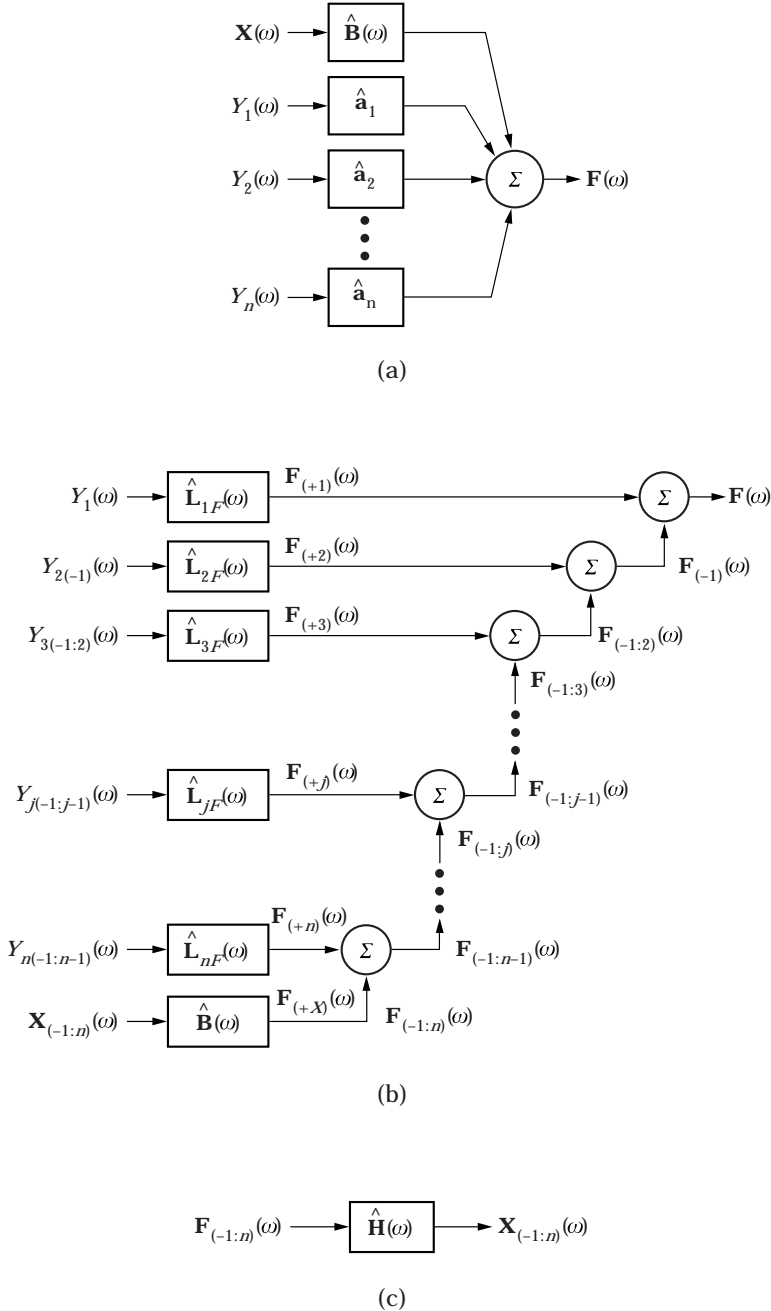


Figure 3. "Reverse path" spectral model. (a) Model with correlated inputs, equation (10). (b) Conditioned model with uncorrelated inputs. (c) "Forward path" of the underlying linear sub-system.

Since frequency domain identification techniques typically identify parameters associated with the linear dynamic compliance matrix $\hat{\mathbf{H}}(\omega) = \hat{\mathbf{B}}(\omega)^{-1}$, or derivatives thereof, the linear path is re-reversed as shown in Figure 3(c). Conditioned frequency response function estimators “ H_{c1} ” and “ H_{c2} ” are now defined as

conditioned “ H_{c1} ” estimate: $[\hat{\mathbf{H}}^{[c1]}(\omega)]^T = \mathbf{G}_{FF(-1:n)}^{-1}(\omega)\mathbf{G}_{FX(-1:n)}(\omega)$,

conditioned “ H_{c2} ” estimate: $[\hat{\mathbf{H}}^{[c2]}(\omega)]^T = \mathbf{G}_{XF(-1:n)}^{-1}(\omega)\mathbf{G}_{XX(-1:n)}(\omega)$, (11a, b)

where $\mathbf{G}_{FF(-1:n)}(\omega)$, $\mathbf{G}_{FX(-1:n)}(\omega)$ and $\mathbf{G}_{XX(-1:n)}(\omega)$ are conditioned spectral density matrices. Calculation of these matrices is discussed by Richards and Singh [7] which is a higher dimensional derivation of the calculation proposed earlier by Bendat and Piersol [6, 16]. Now, modal parameters can be determined from the conditioned estimates (11a) or (11b) without any influence from the non-linearities. The coefficients \hat{a}_j are also recovered as a function of frequency [7], i.e., $\hat{a}_j = \hat{a}_j(\omega)$. Since the true coefficients a_j are constants for Examples I and II, accurate estimates should lead to $\langle \hat{a}_j(\omega) \rangle_\omega = a_j$, where $\langle \cdot \rangle_\omega$ signifies spectral mean.

As will be illustrated in section 4, both Temporal and Spectral Methods successfully estimate the linear properties of Table 1 and the coefficients of the nonlinear elastic force terms of Table 2 when the simulated data set is noise free and the correct model $p_{12}^e(t)$ is chosen to describe the true non-linear elastic force $f_{12}^e(t)$, i.e., $p_{12}^e(t) = f_{12}^e(t)$. However, in practice, experimental data is corrupted by measurement noise, and the nature and mathematical form of $f_{12}^e(t)$ is rarely known. As a result, errors occur in the estimates, especially when measurement noise is significant or when $f_{12}^e(t)$ is poorly represented by $p_{12}^e(t)$; both issues will be discussed in sections 5 and 6. Consequently, two of the specific objectives of this article are to determine when noise levels are tolerable and when an accurate model has been chosen. The latter of these two objectives has previously been addressed by Mohammad *et al.* [10] for the Temporal Method. They determined the response of the estimated model by numerical integration and compared it with the response of the system under identification. However, their method requires the additional computation of the model’s response and a more direct approach is desirable. Consequently, we adopted the Spectral Method as the primary identification method. From the Spectral Method one may take advantage of coherence concepts for measuring the “cause–effect” relationships. These coherence functions may also indicate the frequencies corrupted by the non-linearities, which itself may be useful for designing non-linear elements such as rubber and hydraulic engine mounts [17].

3. COHERENCE FUNCTIONS BASED ON CONDITIONED SPECTRA

Recall the conditioned “reverse path” model of Figure 3(b). Ordinary coherence functions between the conditioned spectra $Y_{j(-1:j-1)}(\omega)$ and excitation $F_1(\omega)$ of $\mathbf{F}(\omega)$ are given as

$$\hat{\gamma}_{jF_1(-1:j-1)}^2(\omega) = \frac{|G_{jF_1(-1:j-1)}(\omega)|^2}{G_{j(-1:j-1)}(\omega)G_{F_1F_1}(\omega)}, \quad 1 \leq j \leq n, \quad (12)$$

where $G_{jF_1(-1:j-1)}(\omega)$ is the conditioned cross-power spectral density function between $Y_{j(-1:j-1)}(\omega)$ and $F_1(\omega)$, $G_{jj(-1:j-1)}(\omega)$ is the conditioned auto-power spectral density function of $Y_{j(-1:j-1)}(\omega)$ and $G_{F_1F_1}(\omega)$ is the unconditioned auto-power spectral density function of the excitation $F_1(\omega)$. Similarly, ordinary coherence functions between each element of $\mathbf{X}_{(-1:n)}(\omega) = [X_{1(-1:n)}(\omega) \ X_{2(-1:n)}(\omega)]^T$ and excitation $F_1(\omega)$ can be calculated by

$$\hat{\gamma}_{X_iF_1(-1:n)}^2(\omega) = \frac{|G_{X_iF_1(-1:n)}(\omega)|^2}{G_{X_iX_i(-1:n)}(\omega)G_{F_1F_1}(\omega)}, \quad i = 1, 2, \tag{13}$$

where $G_{X_iF_1(-1:n)}(\omega)$ is the conditioned cross-power spectral density function between $X_{i(-1:n)}(\omega)$ and $F_1(\omega)$, and $G_{X_iX_i(-1:n)}(\omega)$ is the conditioned auto-power spectral density function of $X_{i(-1:n)}(\omega)$. The coherence functions of equations (12) and (13) are scalar values between 0 and 1 at each frequency and they indicate the amount of contribution from each respective input to the model of Figure 3(b).

Notice in Figure 3(b) that no conditioning is used to uncorrelate the elements $X_{1(-1:n)}(\omega)$ and $X_{2(-1:n)}(\omega)$ of $\mathbf{X}_{(-1:n)}(\omega)$, i.e., the linear component of the response $\mathbf{X}_{(-1:n)}(\omega)$ remains a vector input to the model. Therefore, a multiple coherence function cannot be defined in its conventional form [6, 16] for this model. However, cumulative coherence functions $\hat{\gamma}_{M_i}^2(\omega)$ which include only one of the coherence functions of equation (13) in the summation are defined here as

$$\hat{\gamma}_{M_i}^2(\omega) = \hat{\gamma}_{X_iF_1(-1:n)}^2(\omega) + \hat{\gamma}_{YF_1}^2(\omega), \quad i = 1, 2; \quad \hat{\gamma}_{YF_1}^2(\omega) = \sum_{j=1}^n \hat{\gamma}_{jF_1(-1:j-1)}^2(\omega), \tag{14a, b}$$

which are also scalar values between 0 and 1 at each frequency and may be considered as a measure of the accuracy of the entire model, Figure 3(b). Each coherence function $\hat{\gamma}_{M_i}^2(\omega)$ is given as the sum of two terms. The first term $\hat{\gamma}_{X_iF_1(-1:n)}^2(\omega)$ indicates contribution from the linear spectral component of the response of the i th mass, and the second term $\hat{\gamma}_{YF_1}^2(\omega)$ indicates contribution from the non-linearities. Analysis of $\hat{\gamma}_{X_iF_1(-1:n)}^2(\omega)$ and $\hat{\gamma}_{YF_1}^2(\omega)$ may be useful when it is desired to have non-linearities contributing at certain frequencies, by design [17].

Finally, partial coherence functions are defined for each path of the model of Figure 3(b). However, only the partial coherence functions between the elements of $\mathbf{X}_{(-1:n)}(\omega)$ and $F_{1(-1:n)}(\omega)$ are given here as

$$\hat{\xi}_{X_iF_1(-1:n)}^2(\omega) = \frac{|G_{X_iF_1(-1:n)}(\omega)|^2}{G_{X_iX_i(-1:n)}(\omega)G_{F_1F_1(-1:n)}(\omega)}, \quad i = 1, 2. \tag{15}$$

The partial coherence functions (15) are similar to the ordinary coherence functions (13) with the exception that the denominator of equation (15) contains the conditioned auto-power spectral density function $G_{F_1F_1(-1:n)}(\omega)$. Consequently, $\hat{\xi}_{X_iF_1(-1:n)}^2(\omega)$ are the ordinary coherence functions for the linear sub-system of Figure 3(c). These functions indicate the accuracy of (11a, b), and

$$\hat{\xi}_{X_iF_1(-1:n)}^2(\omega) \approx \frac{|H_{i1}^{[c1]}(\omega)|^2}{|H_{i1}^{[c2]}(\omega)|^2}, \quad i = 1, 2, \tag{16}$$

TABLE 3

Estimated physical properties of Example I by the Temporal Method

Model, noise level	<i>i</i>	\hat{m}_i (kg)	\hat{c}_i (N · s/m)	\hat{k}_i (kN/m)	Estimated coefficients of $y_i(t)$
A ₁ , none	1	1.0 (0.0)	10.0 (0)	100.0 (0.0)	$\hat{a}_3(\omega) = 500.0 \text{ MN/m}^3 (0.0)$
	2	1.0 (0.0)	10.0 (0)	100.0 (0.0)	
A ₁ , moderate	1	1.0 (0.0)	10.0 (0)	100.2 (0.2)	$\hat{a}_3(\omega) = 497.4 \text{ MN/m}^3 (0.5)$
	2	1.0 (0.0)	10.0 (0)	99.7 (0.3)	
A ₁ , high	1	0.8 (20.0)	13.8 (38.0)	118.4 (18.4)	$\hat{a}_3(\omega) = 318.1 \text{ MN/m}^3 (36.4)$
	2	0.7 (30.0)	5.9 (41.0)	75.6 (24.4)	
B ₁ , none	1	0.9 (10.0)	10.9 (9.0)	257.7 (157.7)	$\hat{a}_5(\omega) = 252.7 \text{ GN/m}^5 (-)$
	2	0.9 (10.0)	8.6 (14.0)	93.7 (6.3)	

% Error = (|estimated – true|/true) · 100, given in parentheses.

where the superscripts [c1] and [c2] signify “ H_{c1} ” and “ H_{c2} ” estimates, respectively. Note, equation (16) is an approximation since $\mathbf{F}(\omega) = [F_1(\omega) \ 0]^T$ for Examples I and II, and therefore $\mathbf{G}_{XF(-1:n)}(\omega)$ of equation (11b) is a column vector of dimension 2. Accordingly, this leads to a pseudo-inverse to solve for $[\hat{\mathbf{H}}^{[c2]}(\omega)]^T = [\hat{H}_{11}^{[c2]}(\omega) \ \hat{H}_{21}^{[c2]}(\omega)]$.

4. PRELIMINARY RESULTS

Consider the simulated input/output data of Example I in the absence of uncorrelated noise and assume that the correct Model A₁ of the elastic force $f_{12}^e(t)$ has been chosen:

$$\text{Model A}_1: p_{12}^e(t) = \hat{k}_1 \Delta x_{12}(t) + \hat{a}_3 y_3(\Delta x_{12}(t)) = \hat{k}_1 \Delta x_{12}(t) + \hat{a}_3 \Delta x_{12}(t)^3. \quad (17)$$

From the Temporal Method, the estimated mass, damping and stiffness coefficients and the coefficient \hat{a}_3 of the non-linear function $y_3(\Delta x_{12}(t))$ are listed in Table 3 along with the percentage error of the estimated to true values. As can be seen, the method accurately estimates the system properties. For the sake of comparison, since modal parameters are estimated from equations (11a) or (11b) for the Spectral Method, Table 4 lists modal parameters which are calculated from the mass, damping and stiffness coefficients of Table 3.

Next, the Spectral Method is employed to the data using Model A₁ of equation (17). A sample conditioned “ H_{c2} ” estimate from equation (11b), designated as $\hat{H}_{11}^{[c2]}(\omega)$, is illustrated in Figure 4. Also shown are $\hat{H}_{11}^{[1]}(\omega)$ and $H_{11}(\omega)$. The magnitude and phase are both well estimated by $\hat{H}_{11}^{[c2]}(\omega)$. The underlying linear system’s modal parameters are calculated from the “ H_{c2} ” spectra using a modal parameter estimation software [18]. In Table 5, results and errors between the estimated and true values are listed. As shown, this method has successfully recovered the true linear parameters. Illustrated in Figure 5, is the complex valued $\hat{a}_3(\omega)$ whose trend is constant with frequency. The spectral mean $\langle \hat{a}_3(\omega) \rangle_\omega$ listed in Table 5 suggests some error in the estimate since the true coefficient β_3 is a real

valued constant. However, the real part of the spectral mean is three orders of magnitude greater than the imaginary part and the percentage error between $|\langle \hat{a}_3(\omega) \rangle_\omega|$ and β_3 is less than 1%. For the sake of brevity, the phase spectra of $\mathbf{H}(\omega)$ and $\hat{\mathbf{H}}(\omega)$ as well as the spectra of the estimated coefficients $\hat{a}_j(\omega)$ will be excluded from the remaining results. Unless otherwise mentioned, assume that the results are similar to those presented in Figures 4 and 5. The cumulative coherence function $\hat{\gamma}_{M1}^2(\omega)$ illustrated in Figure 6(a) indicates the overall certainty of the assumed mathematical model. Aside from a minor drop in coherence at the frequency of the first resonance, $\hat{\gamma}_{M1}^2(\omega)$ is unity indicating that an accurate model has been chosen. This is expected since uncorrelated noise is absent and $p_{12}^e(t) = f_{12}^e(t)$ for Model A₁. The coherence functions $\hat{\gamma}_{YF_1}^2(\omega)$ and $\hat{\gamma}_{X_1F_1(-1)}^2(\omega)$ shown in Figure 6(b) illustrate the contribution of the separate paths, i.e., $\hat{\gamma}_{YF_1}^2(\omega)$ shows the contribution of $Y_3(\omega)$ since $y_3(\Delta x_{12}(t))$ is the only non-linear function included in this model, and $\hat{\gamma}_{X_1F_1(-1)}^2(\omega)$ shows contribution of linear component $X_{1(-1)}(\omega)$ of the response $X_1(\omega)$. The coherence function $\hat{\gamma}_{X_1F_1(-1)}^2(\omega)$ peaks in the 50 Hz frequency range and at the upper end of the spectrum, while the coherence function $\hat{\gamma}_{YF_1}^2(\omega)$ of the cubic non-linear function $Y_3(\omega)$ does the opposite. This may be explained as follows. First, $\hat{\gamma}_{YF_1}^2(\omega)$ is high at frequencies corresponding to the peaks of $\hat{H}_{11}^{[e2]}(\omega)$ of Figure 4(a). This suggests that the cubic non-linearity dominates at these frequencies which is understandable since dominant non-linear behavior is expected at frequencies where large amplitudes occur. In contrast, the linear path $X_{1(-1)}(\omega)$ is not as apparent at these frequencies as illustrated by $\hat{\gamma}_{X_1F_1(-1)}^2(\omega)$. However, $\hat{\gamma}_{X_1F_1(-1)}^2(\omega)$ increases in the 50 Hz range as mentioned. This is also understood by examining Figure 4(a). In the 50 Hz range the two estimates $\hat{H}_{11}^{[1]}(\omega)$ and $\hat{H}_{11}^{[e2]}(\omega)$ coincide with $H_{11}(\omega)$. Therefore, $\hat{H}_{11}^{[1]}(\omega)$ is accurate in this frequency range. However, since the conventional “ H_1 ” estimator does not account for non-linearities, the response in this range must be close to the linear behavior. Hence, the reason for an increase in $\hat{\gamma}_{X_1F_1(-1)}^2(\omega)$ values in this range. Although both $\hat{\gamma}_{M1}^2(\omega)$ and $\hat{\gamma}_{M2}^2(\omega)$ are examined for each model, $\hat{\gamma}_{M2}^2(\omega)$ is excluded since both are similar. The ordinary coherence $\hat{\gamma}_{X_2F_1(-1)}^2(\omega)$ which is similar to $\hat{\gamma}_{X_1F_1(-1)}^2(\omega)$ is also excluded for the same reason. The results of this section serve

TABLE 4
Estimated modal properties of Example I by the Temporal Method

Model, noise level	Mode, r	$\hat{\omega}_r$ (Hz)	$\hat{\zeta}_r$ (%)	$\hat{\phi}_r$
A ₁ , none	1	31.1 (0.0)	1.0 (0.0)	{1.0, 0.6}
	2	81.4 (0.0)	2.6 (0.0)	{-0.6, 1.0}
A ₁ , moderate	1	31.1 (0.0)	1.0 (0.0)	{1.0, 0.6}
	2	81.6 (0.2)	2.6 (0.0)	{-0.6, 1.0}
A ₁ , high	1	32.0 (2.9)	0.9 (10.0)	{1.0, 0.7}
	2	96.2 (18.2)	3.3 (26.9)	{-0.7, 1.0}
B ₁ , none	1	33.9 (9.0)	0.9 (10.0)	{1.0, 0.8}
	2	123.8 (52.1)	1.8 (30.8)	{-0.8, 1.0}

% Error = (estimated - true/true) · 100, given in parentheses.

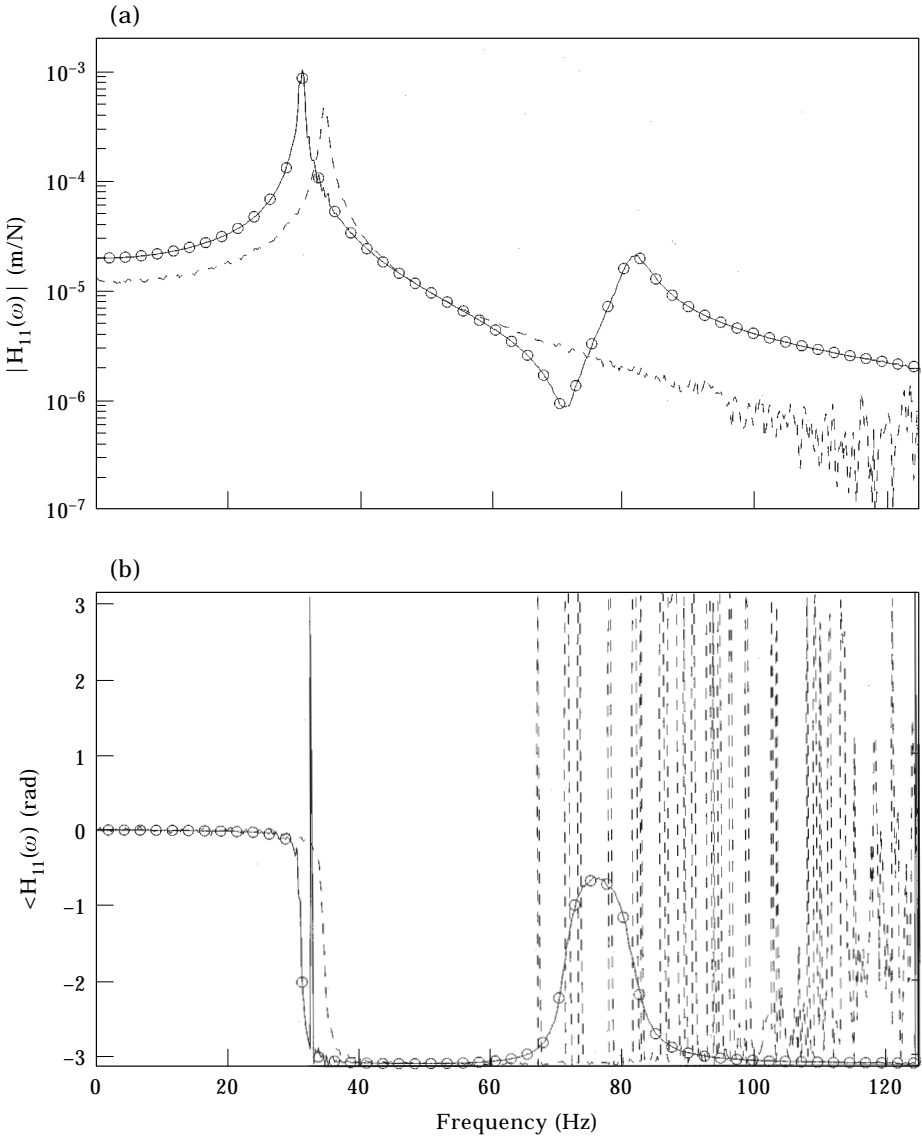


Figure 4. Dynamic compliance spectra of Example I using Model A₁ for “H_{c2}” estimate. (a) Magnitude of H₁₁(ω). (b) Phase of H₁₁(ω). —, $\hat{H}_{11}^{(c2)}(\omega)$; ---, $\hat{H}_{11}^{(1)}(\omega)$; o o o, H₁₁(ω).

as the starting point as other complications are included in the identification scheme.

5. INCLUSION OF UNCORRELATED NOISE

5.1. FORMULATION

In the presence of uncorrelated noise, the response and excitation vectors are modified as

$$\tilde{\mathbf{x}}(t) = \mathbf{x}(t) + \mathbf{n}_x(t), \quad \tilde{\mathbf{f}}(t) = \mathbf{f}(t) + \mathbf{n}_f(t), \quad (18a, b)$$

TABLE 5
Estimated properties of Example I by the Spectral Method

Model, noise level	Mode, r	$\hat{\omega}_r$ (Hz)	$\hat{\zeta}_r$ (%)	$\hat{\phi}_r$	Spectral mean of estimated coefficients of $y_i(t)$
A ₁ , none	1	31.2 (0.3)	1.0 (0.0)	{1.0, 0.6}	$\langle \hat{a}_3(\omega) \rangle_\omega = 501.4 + 0.2i \text{ MN/m}^3$ (0.3)
	2	81.6 (0.2)	2.6 (0.0)	{-0.6, 1.0}	
A ₁ , moderate	1	31.1 (0.0)	1.1 (10.0)	{1.0, 0.6}	$\langle \hat{a}_3(\omega) \rangle_\omega = 496.0 - 8.4i \text{ MN/m}^3$ (1.9)
	2	82.1 (0.9)	1.8 (30.8)	{-0.6, 1.0}	
A ₁ , high	1	32.5 (4.5)	0.1 (90.0)	{1.0, 0.8}	$\langle \hat{a}_3(\omega) \rangle_\omega = 160.8 + 59.7i \text{ MN/m}^3$ (68.9)
	2	- (-)	- (-)	-	
B ₁ , none	1	34.0 (9.3)	1.2 (20.0)	{1.0, 0.8}	$\langle \hat{a}_3(\omega) \rangle_\omega = 251.9 + 0.3i \text{ GN/m}^5$ (-)
	2	118.5 (45.6)	1.6 (38.5)	{-0.8, 1.0}	

% Error = $(\text{estimated} - \text{true}/\text{true}) \cdot 100$, given in parentheses.

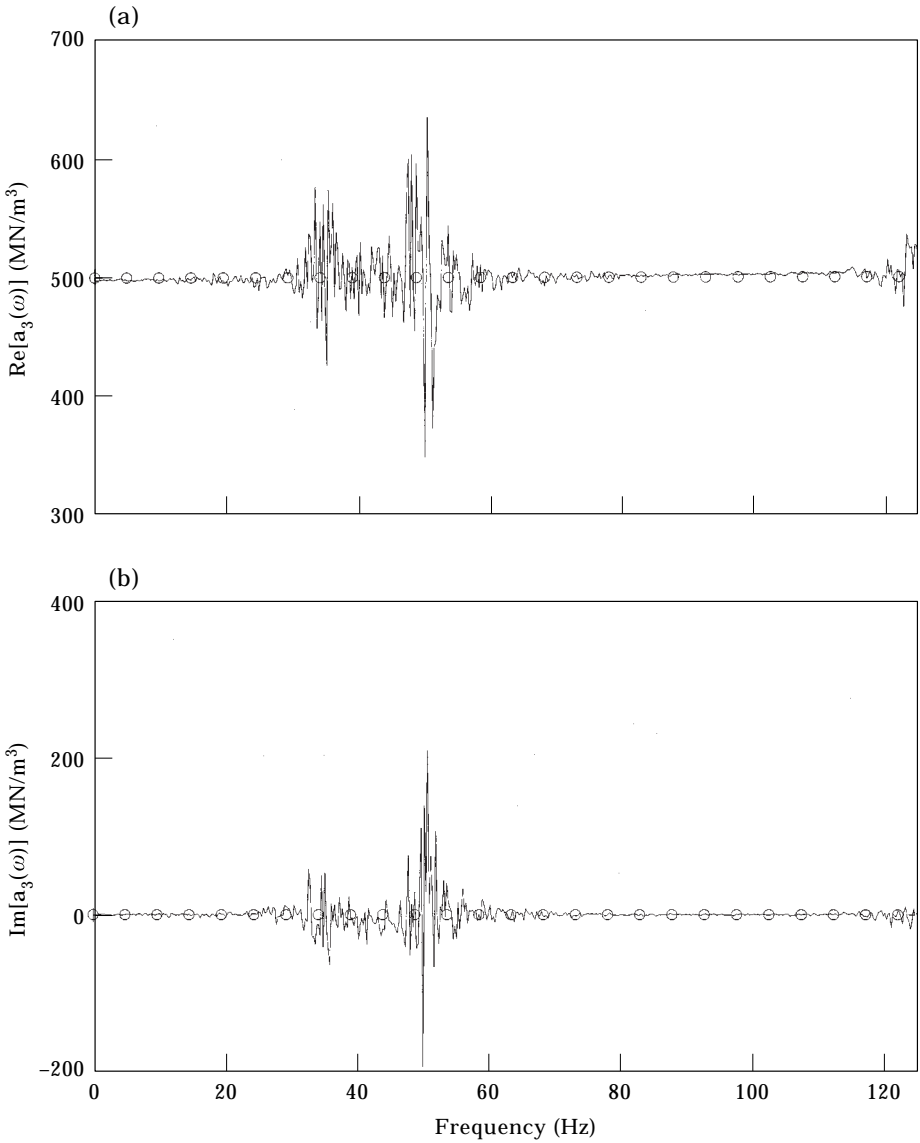


Figure 5. Spectrum of estimated coefficient $\hat{a}_3(\omega)$ of Model A_1 . (a) $\text{Re}[\hat{a}_1(\omega)]$. (b) $\text{Im}[\hat{a}_1(\omega)]$. —, $\hat{a}_3(\omega)$; ○○○, true coefficient β_3 .

where $\tilde{\mathbf{x}}(t)$ is the contaminated response vector of the true response vector $\mathbf{x}(t)$ by uncorrelated noise vector $\mathbf{n}_x(t)$. Likewise, $\tilde{\mathbf{f}}(t)$ is the contaminated excitation vector of the true excitation vector $\mathbf{f}(t)$ by uncorrelated noise vector $\mathbf{n}_f(t)$. The Fourier transform $\mathbf{F}[\cdot]$ of equations (18a, b) leads to

$$\tilde{\mathbf{X}}(\omega) = \mathbf{X}(\omega) + \mathbf{N}_x(\omega), \quad \tilde{\mathbf{F}}(\omega) = \mathbf{F}(\omega) + \mathbf{N}_f(\omega) \quad (19a, b)$$

and since $\mathbf{N}_X(\omega)$ and $\mathbf{N}_F(\omega)$ are uncorrelated noise spectra,

$$\mathbf{G}_{XN_X}(\omega) = \frac{2}{T} E[\mathbf{X}(\omega)^* \cdot \mathbf{N}_X(\omega)^T] = \mathbf{0}, \quad \mathbf{G}_{XN_F}(\omega) = \frac{2}{T} E[\mathbf{X}(\omega)^* \cdot \mathbf{N}_F(\omega)^T] = \mathbf{0},$$

$$\mathbf{G}_{FN_X}(\omega) = \frac{2}{T} E[\mathbf{F}(\omega)^* \cdot \mathbf{N}_X(\omega)^T] = \mathbf{0}, \quad \mathbf{G}_{FN_F}(\omega) = \frac{2}{T} E[\mathbf{F}(\omega)^* \cdot \mathbf{N}_F(\omega)^T] = \mathbf{0},$$

$$\mathbf{G}_{N_X N_F}(\omega) = \frac{2}{T} E[\mathbf{N}_X(\omega)^* \cdot \mathbf{N}_F(\omega)^T] = \mathbf{0}, \quad (20a-e)$$

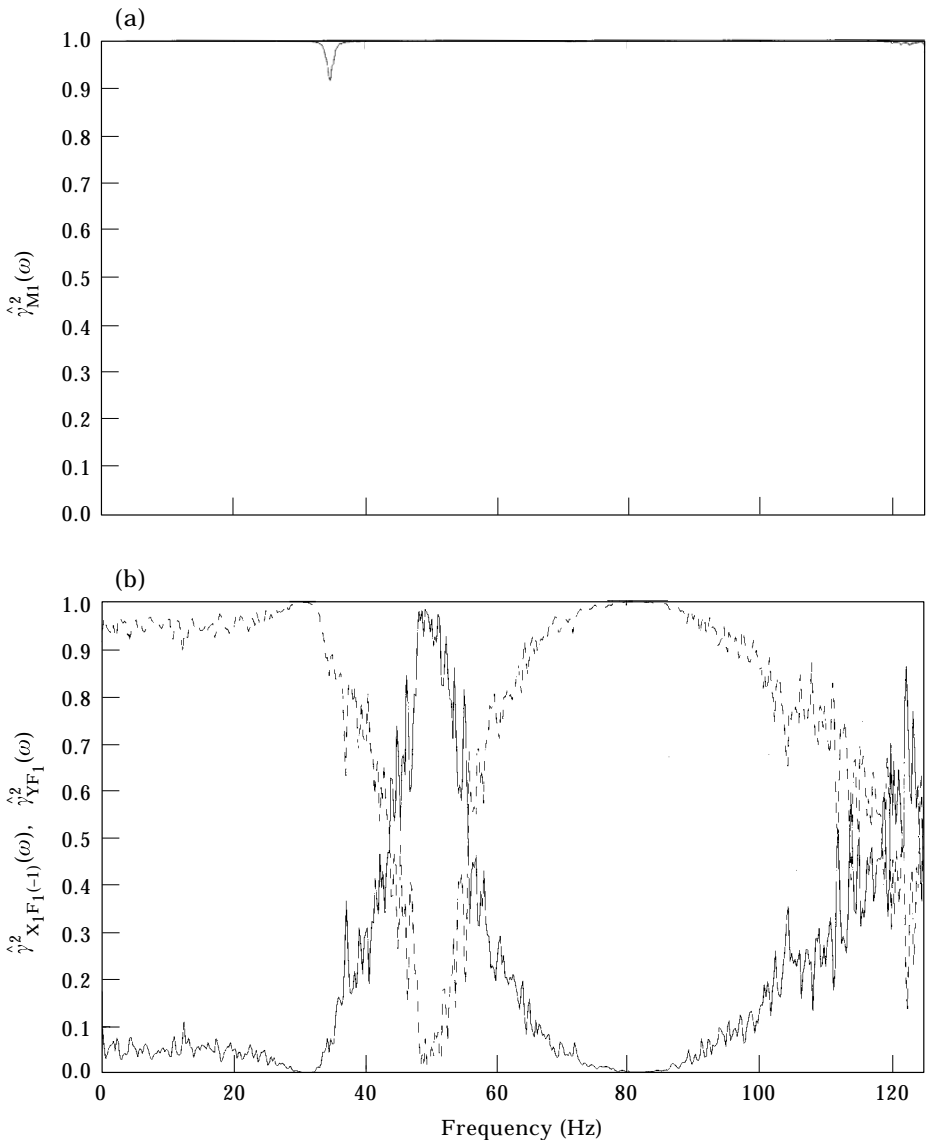


Figure 6. Coherence functions of Model A1. (a) Cumulative coherence function $\hat{\gamma}_{M1}^2(\omega)$. (b) Coherence functions $\hat{\gamma}_{X_1 F_1(-1)}^2(\omega)$ and $\hat{\gamma}_{Y F_1}^2(\omega)$. —, $\hat{\gamma}_{X_1 F_1(-1)}^2(\omega)$; ---, $\hat{\gamma}_{Y F_1}^2(\omega)$.

where $\mathbf{0}$ is a square null matrix of dimension 2. However,

$$\lceil \mathbf{G}_{N_X N_X}(\omega) \rceil = \frac{2}{T} E[\mathbf{N}_X(\omega)^* \cdot \mathbf{N}_X(\omega)^T] \neq \mathbf{0},$$

$$\lceil \mathbf{G}_{N_F N_F}(\omega) \rceil = \frac{2}{T} E[\mathbf{N}_F(\omega)^* \cdot \mathbf{N}_F(\omega)^T] \neq \mathbf{0}, \tag{21a, b}$$

where $\lceil \mathbf{G}_{N_X N_X}(\omega) \rceil$ and $\lceil \mathbf{G}_{N_F N_F}(\omega) \rceil$ are square diagonal matrices of dimension 2. When conventional frequency response estimators are employed, noise only exists in the auto-power spectra of $\tilde{\mathbf{X}}(\omega)$ and $\tilde{\mathbf{F}}(\omega)$. However, when calculating the conditioned estimates of equations (11a, b), noise exists in additional spectra, as follows. The noise $\mathbf{n}_x(t)$ contaminates the n unique non-linear functions $y_j(\Delta x_{12}(t))$ since they are calculated directly from the contaminated response $\tilde{\mathbf{x}}(t)$, i.e.,

$$\tilde{y}_j = \tilde{y}_j(\Delta \tilde{x}_{12}(t)),$$

$$\Delta \tilde{x}_{12}(t) = \tilde{x}_1(t) - \tilde{x}_2(t) = x_1(t) + n_{x_1}(t) - x_2(t) - n_{x_2}(t) = \Delta x_{12}(t) + \Delta n_x(t),$$

$$\Delta n_x(t) = n_{x_1}(t) - n_{x_2}(t). \tag{22a-c}$$

Since the functions $\tilde{y}_j(\Delta \tilde{x}_{12}(t))$ are of the polynomial form, they can be written as

$$\tilde{y}_j(\Delta \tilde{x}_{12}(t)) = y_j(\Delta x_{12}(t)) + n_{y_j}(t), \quad y_j(\Delta x_{12}(t)) = y_j(\mathbf{x}(t)),$$

$$n_{y_j}(t) = n_{y_j}(\mathbf{x}(t), \mathbf{n}_x(t)), \tag{23a-c}$$

where $\tilde{y}_j(\Delta \tilde{x}_{12}(t))$ is grouped into a term which is only a function of $\mathbf{x}(t)$ without noise and a term which is a function of $\mathbf{x}(t)$ and $\mathbf{n}_x(t)$. To assimilate equations (23a-c) consider a cubic function $y_3(\Delta x_{12}(t)) = \Delta x_{12}(t)^3$ calculated from the contaminated response $\tilde{\mathbf{x}}(t)$:

$$\begin{aligned} \tilde{y}_3(\Delta \tilde{x}_{12}(t)) &= (\Delta \tilde{x}_{12}(t))^3 = (\Delta x_{12}(t) + \Delta n_x(t))^3 \\ &= \Delta x_{12}(t)^3 + 3\Delta x_{12}(t)^2 \Delta n_x(t) + 3\Delta x_{12}(t) \Delta n_x(t)^2 + \Delta n_x(t)^3 \\ &= y_3(\Delta x_{12}(t)) + n_{y_3}(t), \end{aligned}$$

$$n_{y_3}(t) = 3\Delta x_{12}(t)^2 \Delta n_x(t) + 3\Delta x_{12}(t) \Delta n_x(t)^2 + \Delta n_x(t)^3. \tag{24a, b}$$

As shown, $\tilde{y}_3(\Delta \tilde{x}_{12}(t))$ is arranged into a term which is only a function of $\mathbf{x}(t)$ without noise and a term which is a function of $\mathbf{x}(t)$ and $\mathbf{n}_x(t)$. This procedure can be extended to $\tilde{y}_j(\Delta \tilde{x}_{12}(t))$ of any polynomial order j . The Fourier transform $\mathbf{F}[\cdot]$ of equation (23a) leads to

$$\tilde{Y}_j(\omega) = Y_j(\omega) + N_j(\omega), \quad Y_j(\omega) = \mathbf{F}[y_j(\Delta x_{12}(t))], \quad N_j(\omega) = \mathbf{F}[n_{y_j}(t)] \tag{25a-c}$$

and as a result of equations (23b) and (23c),

$$\begin{aligned} \mathbf{G}_{X_j}(\omega) &= \frac{2}{T} E[\mathbf{X}(\omega)^* \cdot Y_j(\omega)] \neq \{0\}, & \mathbf{G}_{XN_j}(\omega) &= \frac{2}{T} E[\mathbf{X}(\omega)^* \cdot N_j(\omega)] \neq \{0\}, \\ \mathbf{G}_{N_X N_j}(\omega) &= \frac{2}{T} E[\mathbf{N}_X(\omega)^* \cdot N_j(\omega)] \neq \{0\}, & G_{jN_j}(\omega) &= \frac{2}{T} E[Y_j(\omega)^* \cdot N_j(\omega)] \neq 0, \\ \mathbf{G}_{N_X j}(\omega) &= \frac{2}{T} E[\mathbf{N}_X(\omega)^* \cdot Y_j(\omega)] = \{0\}, & G_{N_j N_j}(\omega) &= \frac{2}{T} E[N_j(\omega)^* \cdot N_j(\omega)] \neq 0, \end{aligned} \quad (26a-f)$$

where $\{0\}$ are null column vectors of dimension 2. Note that equations (26a-f) are true in a general sense; however, depending on the form of $y_j(\Delta x_{12}(t))$, some of the spectral density functions may be zero. Therefore, equations (26a-f) give the worst possible case. Also, in general components of $\tilde{Y}_j(\omega)$ and $\tilde{Y}_i(\omega)$ may be correlated depending on the form of $\tilde{y}_j(\Delta \tilde{x}_{12}(t))$ and $\tilde{y}_i(\Delta \tilde{x}_{12}(t))$,

$$\begin{aligned} G_{ij}(\omega) &= \frac{2}{T} E[Y_i(\omega)^* \cdot Y_j(\omega)] \neq 0, & G_{iN_j}(\omega) &= \frac{2}{T} E[Y_i(\omega)^* \cdot N_j(\omega)] \neq 0, \\ G_{N_j}(\omega) &= \frac{2}{T} E[N_i(\omega)^* \cdot Y_j(\omega)] \neq 0, & G_{N_i N_j}(\omega) &= \frac{2}{T} E[N_i(\omega)^* \cdot N_j(\omega)] \neq 0. \end{aligned} \quad (27a-d)$$

Consequently, from equations (20a-e), (21a, b), (26a-f) and (27a-d),

$$\begin{aligned} \tilde{\mathbf{G}}_{XX}(\omega) &= \mathbf{G}_{XX}(\omega) + \lceil \mathbf{G}_{N_X N_X}(\omega) \rceil, & \tilde{\mathbf{G}}_{XF}(\omega) &= \mathbf{G}_{XF}(\omega), \\ \tilde{\mathbf{G}}_{X_j}(\omega) &= \mathbf{G}_{X_j}(\omega) + \mathbf{G}_{XN_j}(\omega) + \mathbf{G}_{N_X N_j}(\omega), & \tilde{\mathbf{G}}_{FF}(\omega) &= \mathbf{G}_{FF}(\omega) + \lceil \mathbf{G}_{N_F N_F}(\omega) \rceil, \\ \tilde{\mathbf{G}}_{F_j}(\omega) &= \mathbf{G}_{F_j}(\omega), & \tilde{G}_{ij}(\omega) &= \tilde{G}_{ij}(\omega) + 2 \operatorname{Re} [\tilde{G}_{jN_j}(\omega)] + \tilde{G}_{N_j N_j}(\omega), \\ \tilde{G}_{ij}(\omega) &= G_{ij}(\omega) + G_{iN_j}(\omega) + G_{N_j}(\omega) + G_{N_i N_j}(\omega). \end{aligned} \quad (28a-g)$$

As given by equations (28a-g), noise corrupts most of these unconditioned spectral functions and matrices. As a result, noise also contaminates conditioned spectral density functions used to calculate “ H_{c1} ” and “ H_{c2} ” estimates of equations (11a, b) and the coherence functions of section 3 since conditioned spectra are calculated from equations 28(a-g). Additional research is needed in order to minimize the presence of noise in equations (28a-g) by considering a reference approach [19] which yields an improved estimate of auto-power spectral density functions.

For the Temporal Method, similar problems occur when uncorrelated noise is present since the non-linear functions $\tilde{y}_j(\Delta \tilde{x}_{12}(t))$ are calculated directly from the contaminated response $\tilde{\mathbf{x}}(t)$. Increasing the length of time series utilized by the Temporal Method minimizes contamination of uncorrelated noise since the method is based on a least squares solution. Alternatively, time domain averaging operations may be performed or cross-correlation techniques may be adapted. This is suggested as a topic for future research.

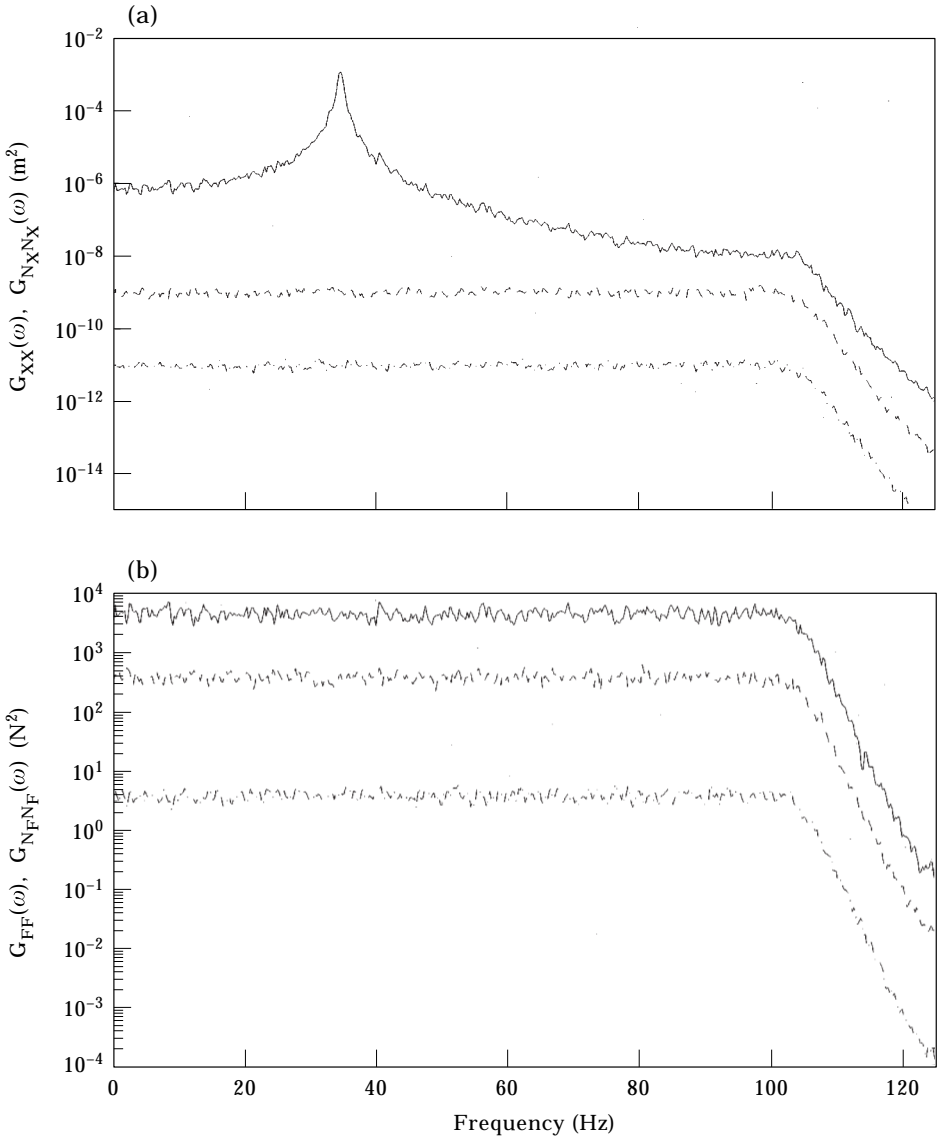


Figure 7. Auto-power spectra of noise-free data, moderate and high noise levels. (a) Response auto-power spectra. (b) Excitation auto-power spectra. —, Noise-free data; ---, high noise level; - · - ·, moderate noise level.

5.2. RESULTS

Both methods are evaluated next by adding “white” uncorrelated noise to the simulated excitation and response data. The auto-power spectra of $X_1(\omega)$, $F_1(\omega)$, $N_{X_1}(\omega)$ and $N_{F_1}(\omega)$ are shown in Figure 7; those of $X_2(\omega)$ and $N_{X_2}(\omega)$ are not shown since they are similar to those of $X_1(\omega)$ and $N_{X_1}(\omega)$. These noise levels are comparable to those used by Mohammad *et al.* [10] and Yang and Ibrahim [11] in their studies based on the Temporal Method. The correct non-linear form is assumed for this study, i.e., equation (17). Shown in Figure 8 are sample dynamic

compliance functions $\hat{H}_{21}^{(c2)}(\omega)$, $\hat{H}_{11}^{(1)}(\omega)$ and $H_{11}(\omega)$. For the moderate noise case the second resonant peak of $\hat{H}_{21}^{(c2)}(\omega)$ reveals some noise corruption, as shown in Figure 8(a). Estimated parameters are listed in Tables 3–5 based on both methods. As shown, not much error has occurred in these estimates with the exception of ζ_2 by the Spectral Method. However, for the high noise case, estimates are rather poor, as shown in Figure 8(b) and listed in Tables 3–5. In fact, since the second mode of the “ H_{c2} ” estimates are undetectable, no parameters can be determined for this mode by the Spectral Method. Illustrated in Figure 9 are $\hat{\gamma}_{M1}^2(\omega)$ for the two noise levels. The large amount of noise responsible for the inaccurate identification in the high noise case is indicated by $\hat{\gamma}_{M1}^2(\omega)$ of Figure 9(b). This

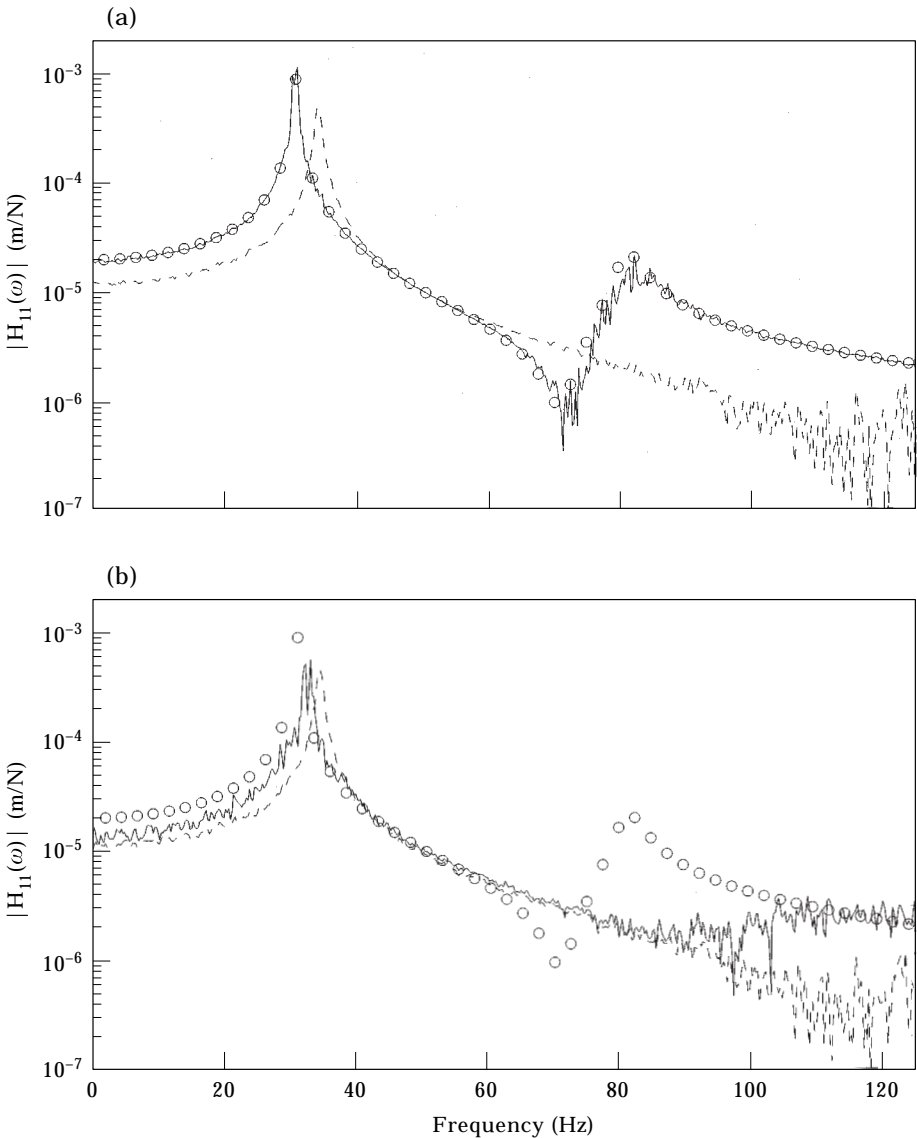


Figure 8. Magnitude of dynamic compliance spectra of Example I using Model A₁ for “ H_{c2} ” estimate. (a) Moderate noise case. (b) High noise case. —, $\hat{H}_{21}^{(c2)}(\omega)$; ---, $\hat{H}_{11}^{(1)}(\omega)$; ○○○, $H_{11}(\omega)$.

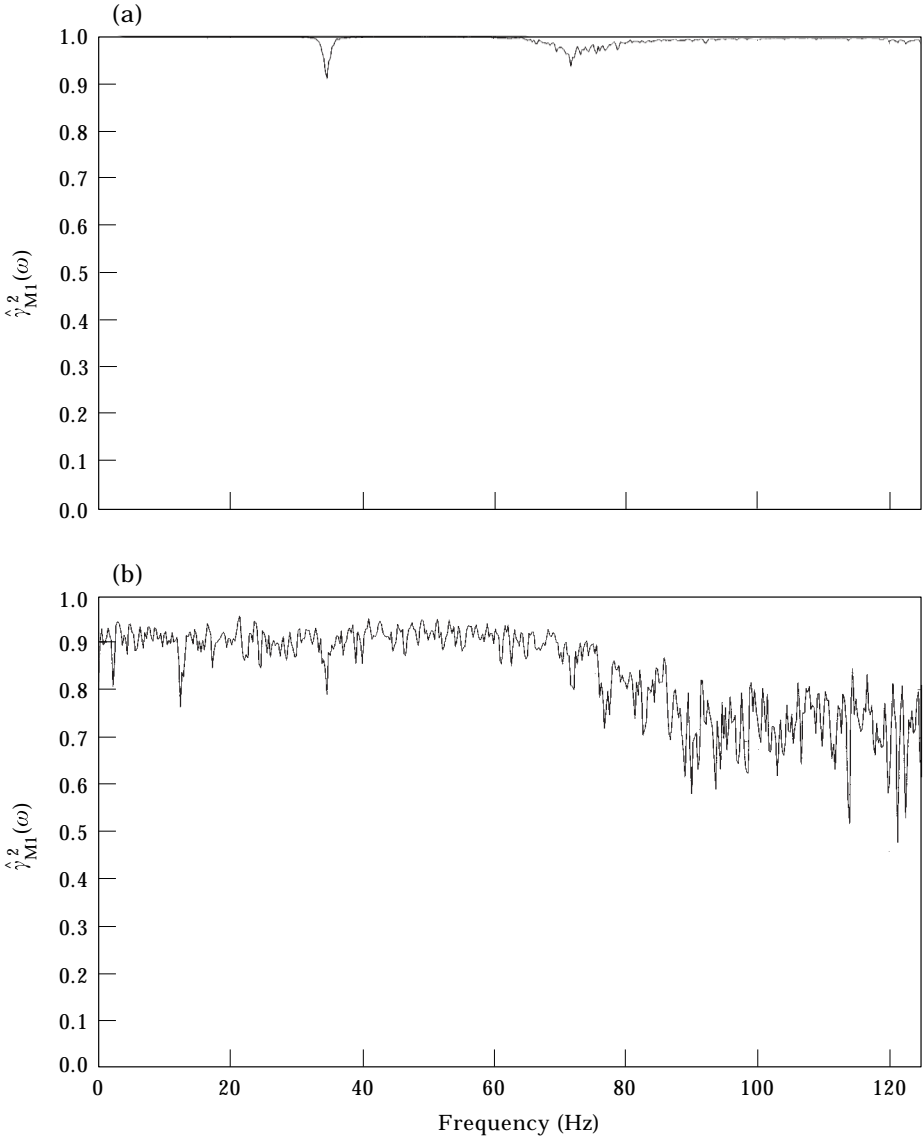


Figure 9. Cumulative coherence functions $\hat{\gamma}_{M1}^2(\omega)$ of Model A_1 . (a) Moderate noise case. (b) High noise case.

suggests that the coherence techniques can in fact aid in determining when noise levels are intolerable.

To this point no results for “ H_{c1} ” estimates based on equation (11a) or partial coherence functions as defined by equation (15) have been shown. These estimates can also be investigated; however, they may be corrupted by the numerical errors introduced by simulating the lightly damped systems, i.e., Examples I and II. To minimize these errors, the damping coefficients of Example I are increased by a factor of 10 to form a new Example III. Applying the Spectral Method with Model A_{III} which takes the same form as A_1 of equation (17), conditioned “ H_{c1} ” and “ H_{c2} ” estimates are calculated in the absence of uncorrelated noise. Shown in Figures 10

and 11 are $\hat{H}_{11}^{[e2]}(\omega)$, $\hat{H}_{11}^{[e1]}(\omega)$, $\hat{H}_{11}^{[1]}(\omega)$, $H_{11}(\omega)$ and $\xi_{X_1 F_1(-1:m)}^2(\omega)$. Some numerical errors still exist since $\hat{H}_{11}^{[e2]}(\omega) \neq \hat{H}_{11}^{[e1]}(\omega)$ and $\xi_{X_1 F_1(-1:m)}^2(\omega)$ drops below unity at the first resonance peak. However, in the absence of noise both $\hat{H}_{11}^{[e2]}(\omega)$ and $\hat{H}_{11}^{[e1]}(\omega)$ are accurate estimates.

The conditioned “ H_{c1} ” and “ H_{c2} ” estimates, as proposed in equations (11a, b), are analogous to the conventional “ H_1 ” and “ H_2 ” estimates currently used for linear systems [2, 3]. Therefore, intuition may lead one to expect the “ H_{c2} ” estimate to perform better than the “ H_{c1} ” estimate in the presence of uncorrelated noise only in the excitation and none in the response. Likewise, one would expect the “ H_{c1} ” estimate to perform better than the “ H_{c2} ” estimate in the presence of

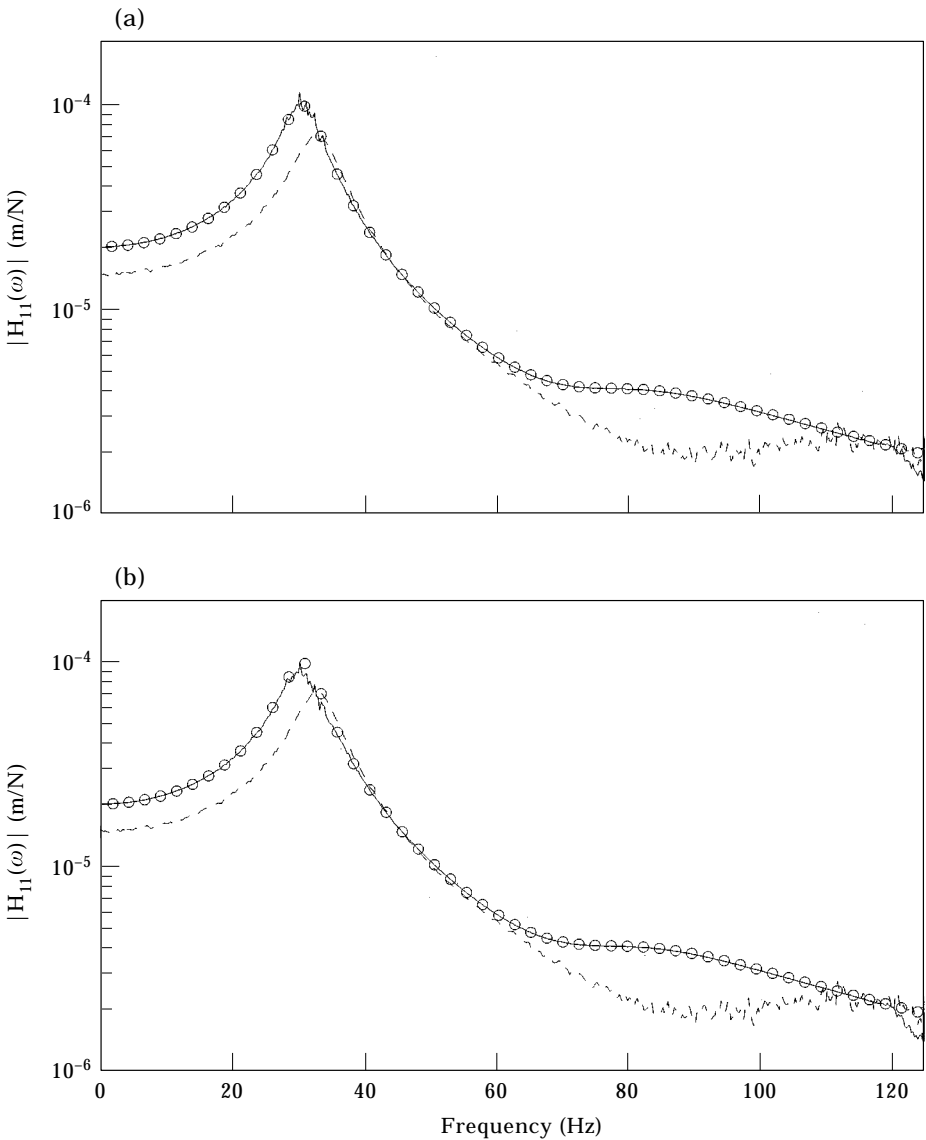


Figure 10. Magnitude of dynamic compliance spectra of Example III using Model A_{III} for “ H_{c2} ” estimate. (a) —, $\hat{H}_{11}^{[e2]}(\omega)$; ---, $\hat{H}_{11}^{[1]}(\omega)$; ○○○, $H_{11}(\omega)$. (b) —, $\hat{H}_{11}^{[e1]}(\omega)$; ---, $\hat{H}_{11}^{[1]}(\omega)$; ○○○, $H_{11}(\omega)$.

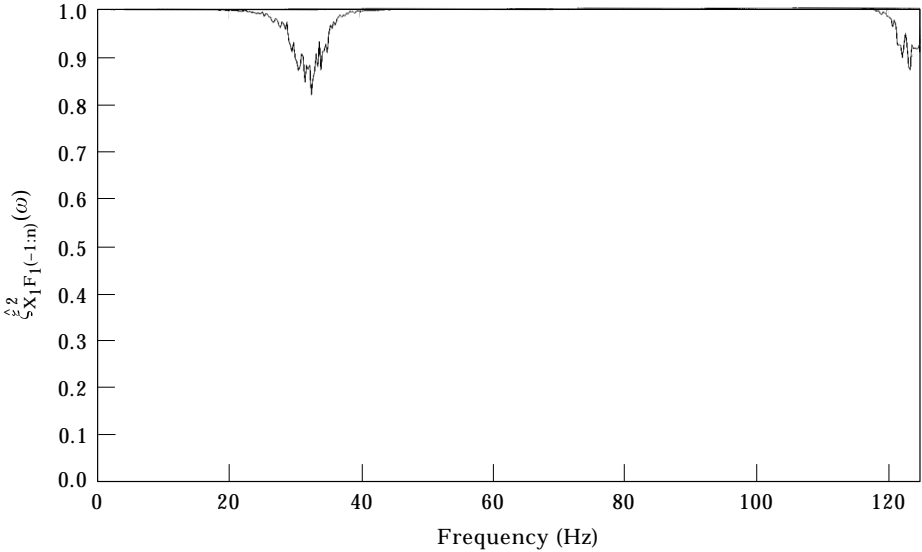


Figure 11. Partial coherence function $\hat{\xi}_{X_1 F_1(-1:m)}^2(\omega)$ of Model A_{III}.

uncorrelated noise only in the response and none in the excitation. To illustrate this, $\hat{H}_{11}^{[c2]}(\omega)$, $\hat{H}_{11}^{[c1]}(\omega)$ and $H_{11}(\omega)$ are illustrated in Figure 12(a) for a high level of uncorrelated noise in the excitation only. As expected, although the results are still “noisy”, $\hat{H}_{11}^{[c2]}(\omega)$ is the better estimate. Figure 12(b) illustrates the same estimates for high levels of uncorrelated noise in the responses only. Unlike what was expected, the “ H_{c2} ” method is still a slightly better estimate. This outcome may be a result of the conditioning required to calculate the “ H_{c1} ” and “ H_{c2} ” estimates. However, this issue requires additional examination in future experimental studies.

6. EXAMINATION OF ALTERNATIVE NON-LINEAR MODELS

The following results illustrate the consequences of identification when alternate formulae are chosen to describe the elastic behavior of the non-linear spring element, i.e., either correct ($p_{12}^e(t) = f_{12}^e(t)$), incorrect ($p_{12}^e(t) \neq f_{12}^e(t)$) or approximate ($p_{12}^e(t) \approx f_{12}^e(t)$) mathematical models will be employed. Due to the heavy damping of the second mode, Example III of section 5.2 will not be evaluated in the following results since it is difficult to determine how well the second mode is estimated by the Spectral Method. Therefore, only Examples I and II will be investigated. As a consequence, since numerical errors resulting from the simulations of Examples I and II corrupt the “ H_{c1} ” estimates of equation (11a) and partial coherence functions of equation (15), only “ H_{c2} ” estimates of equation (11b), $\hat{\gamma}_{M1}^2(\omega)$ and $\hat{\gamma}_{YF_1}^2(\omega)$ of equations (14a, b) will be shown. Finally, since the effects of noise on both Temporal and Spectral Methods have already been examined, data for the following studies are noise free for the sake of maintaining a clear focus on results with alternative models.

6.1. IDENTIFICATION OF EXAMPLE I

Recall, in section 4 where both Temporal and Spectral Methods successfully identify Example I using Model A_I of equation (17) which correctly models $f_{12}^e(t)$. Now assume that the form of the non-linearity $f_{12}^e(t)$ is incorrectly modelled as a linear and fifth order polynomial:

$$\text{Model B}_I: p_{12}^e(t) = k_1 \Delta x_{12}(t) + a_5 y_5^5(\Delta x_{12}(t)) = k_1 \Delta x_{12}(t) + a_5 \Delta x_{12}^5(t). \quad (29)$$

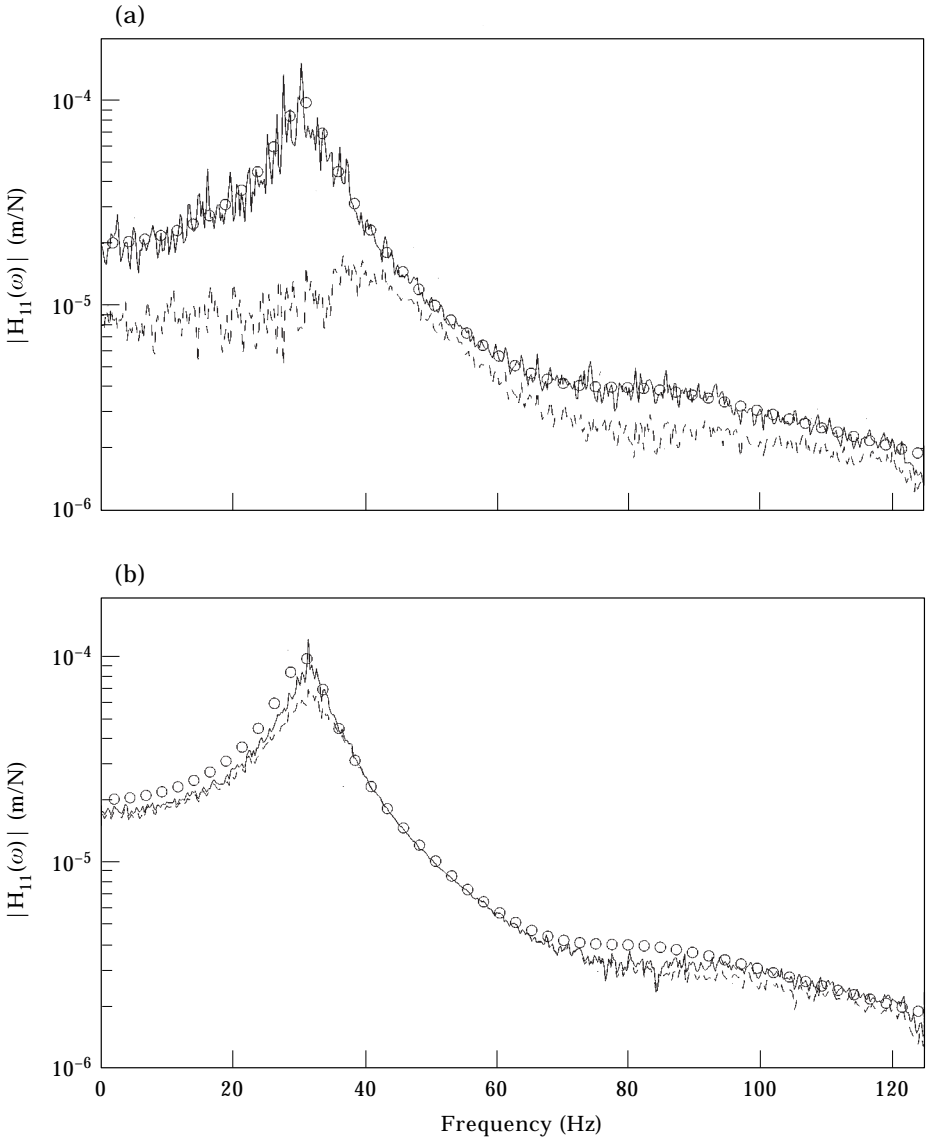


Figure 12. Magnitude of dynamic compliance spectra of Example III using Model A_{III} for Spectral Method calculations. (a) High noise level in excitation only. (b) High noise level in response only. —, $\hat{H}_{11}^{e2}(\omega)$; ---, $\hat{H}_{11}^{e1}(\omega)$; ○○○, $H_{11}(\omega)$.

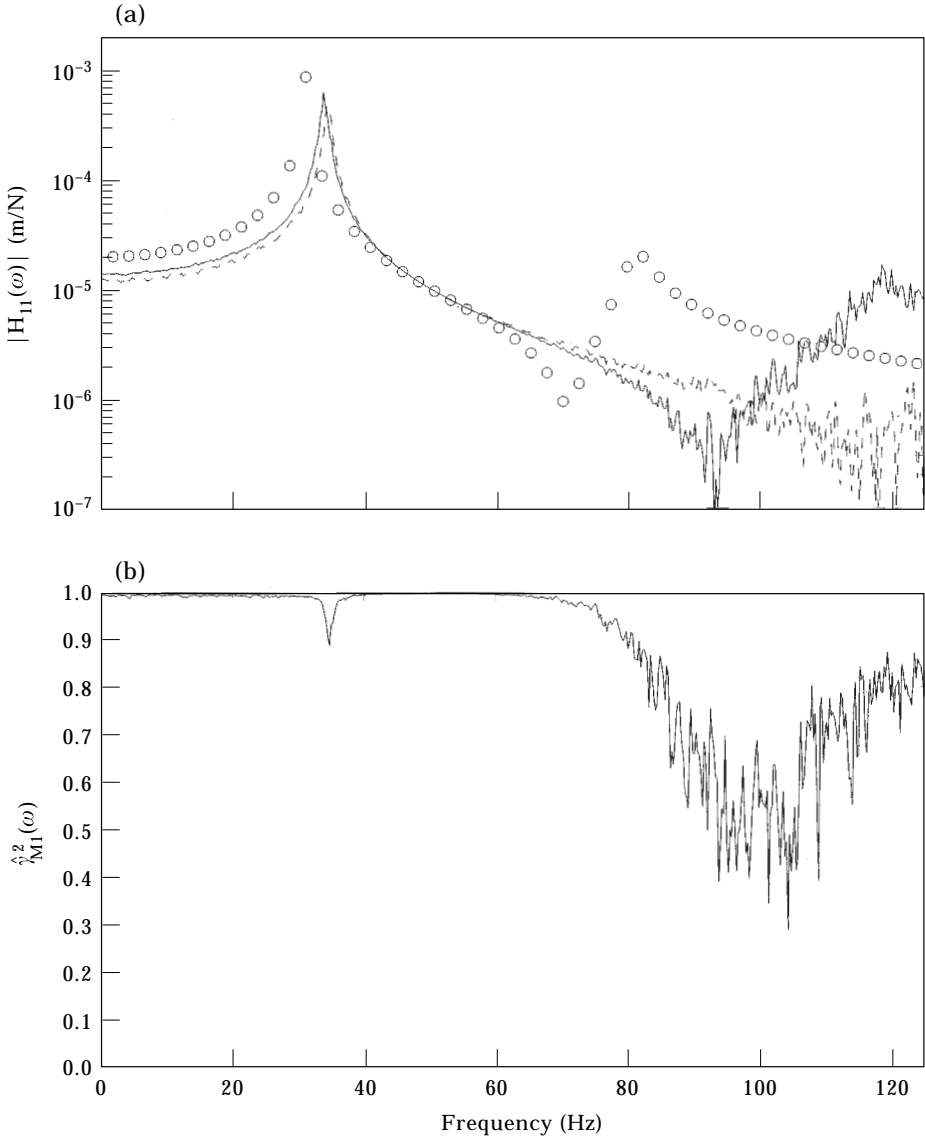


Figure 13. Spectra for Example I using Model B_1 for Spectral Method calculations. (a) Magnitude of $H_{11}(\omega)$. —, $\hat{H}_{11}^{(2)}(\omega)$; ---, $\hat{H}_{11}^{(1)}(\omega)$; $\circ\circ\circ$, $H_{11}(\omega)$. (b) Cumulative coherence function $\hat{\gamma}_{M1}^2(\omega)$.

The procedures of section 4 are again carried through here for both methods and results are given in Tables 3–5 and in Figure 13(a). As shown, the estimates are rather poor. However, without knowing the true parameters, one may not be able to conclude that Model B_1 is incorrect. This acknowledges the importance of diagnostic tools to determine the validity of the models, such as the cumulative coherence function $\hat{\gamma}_{M1}^2(\omega)$ of Figure 13(b). As $\hat{\gamma}_{M1}^2(\omega)$ indicates, B_1 is an inaccurate model above 70 Hz. However, $\hat{\gamma}_{M1}^2(\omega)$ is near unity elsewhere. This may lead one to believe B_1 is accurate below 70 Hz, when in fact the first mode of $\hat{H}_{11}^{(2)}(\omega)$ is shifted to a higher frequency than the true natural frequency. Therefore, in order to prevent this misinterpretation and to ensure that the best possible model is

chosen, cumulative coherence functions $\hat{\gamma}_{M1}^2(\omega)$ of several models should be compared. Doing so with $\hat{\gamma}_{M1}^2(\omega)$ of Models A₁ and B₁ indicates that A₁ is more accurate.

Observe that both Temporal and Spectral Methods give similar results, suggesting that erroneous estimates resulting from an incorrect non-linear model are not method dependent. Subsequently, results to follow will include only those from the Spectral Method, but any dramatic differences between estimates obtained from the two methods will be mentioned.

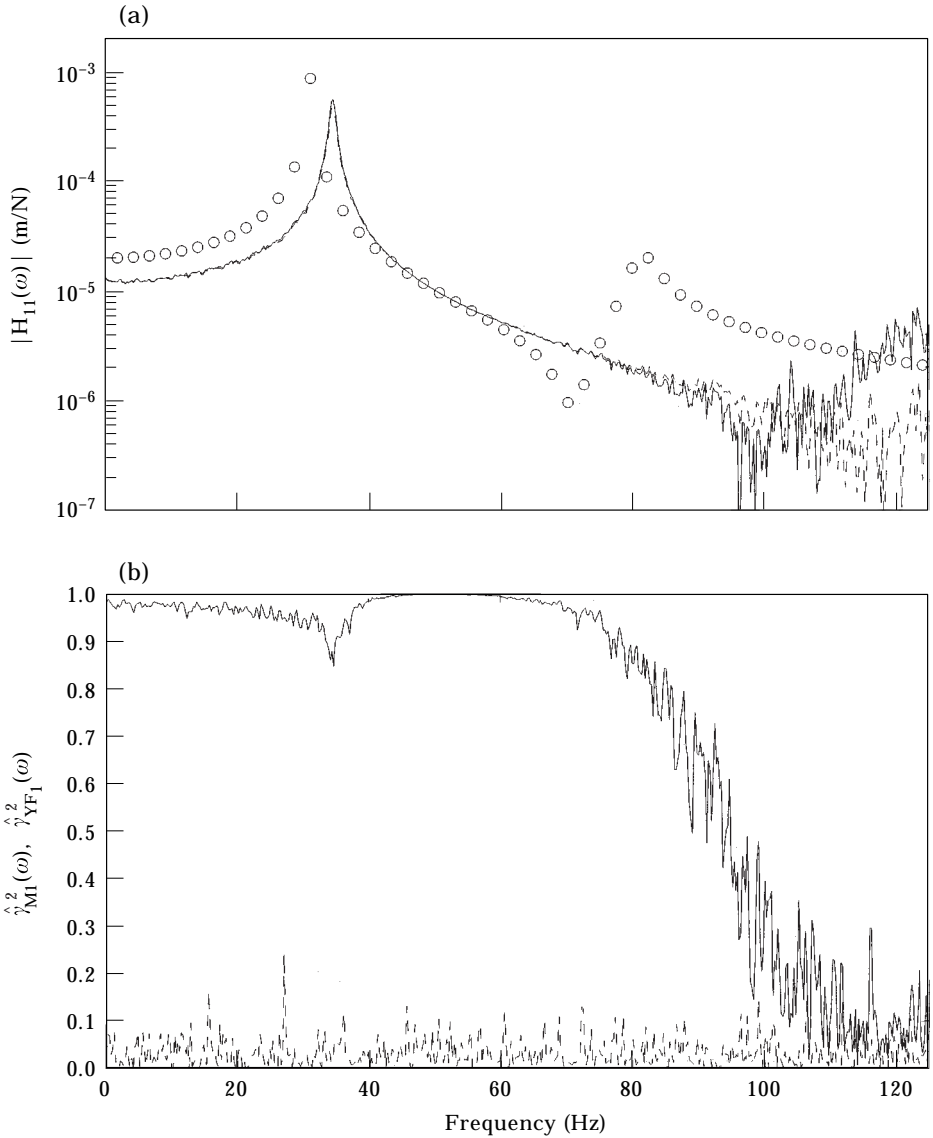


Figure 14. Spectra for Example I using Model C₁ for Spectral Method calculations. (a) Magnitude of $H_{11}(\omega)$. —, $\hat{H}_{11}^{(2)}(\omega)$; ---, $\hat{H}_{11}^{(1)}(\omega)$; ○○○, $H_{11}(\omega)$. (b) Coherence functions $\hat{\gamma}_{M1}^2(\omega)$ and $\hat{\gamma}_{YF_1}^2(\omega)$. —, $\hat{\gamma}_{M1}^2(\omega)$; ---, $\hat{\gamma}_{YF_1}^2(\omega)$.

Next consider Model C₁ which assumes that $f_{12}^e(t)$ contains a quadratic term:

$$\text{Model C}_1: p_{12}^e(t) = k_1 \Delta x_{12}(t) + a_2 y_2(\Delta x_{12}(t)) = k_1 \Delta x_{12}(t) + a_2 x_{12}^2(t). \quad (30)$$

Physically, this type of non-linearity represents a spring with hardening stiffness in tension and softening stiffness in compression when $a_2 > 0$, and vice versa when $a_2 < 0$. Estimates $\hat{H}_{11}^{[1]}(\omega)$, $\hat{H}_{11}^{[c2]}(\omega)$ and true $H_{11}(\omega)$ are shown in Figure 14(a). The two estimates are similar but deviate from the true $H_{11}(\omega)$ suggesting that Model C₁ does not improve the identification over a similar but linear model. The cumulative coherence $\hat{\gamma}_{M1}^2(\omega)$ exceeds 0.85 up to approximately 70 Hz, then it drops off as shown in Figure 14(b). Comparing $\hat{\gamma}_{M1}^2(\omega)$ of Models A₁, B₁ and C₁, indicates that C₁ is the least accurate model chosen thus far, and the coherence function $\hat{\gamma}_{YF_1}^2(\omega)$ also shown in Figure 14(b) is poor at all frequencies, indicating that the quadratic term adds zero contribution to the model. Hence, this is the reason why $\hat{H}_{11}^{[1]}(\omega)$ and $\hat{H}_{11}^{[c2]}(\omega)$ are similar. However, in the small band between 45 and 55 Hz the cumulative coherence is close to unity. This is due to the fact that $\hat{H}_{11}^{[c2]}(\omega)$ and $H_{11}(\omega)$ coincide in this range, as shown in Figure 14(a). Therefore, even such an incorrect model yields an accurate representation in this frequency range.

The next Model D₁ includes both a quadratic and cubic term:

$$\begin{aligned} \text{Model D}_1: p_{12}^e(t) &= k_1 \Delta x_{12}(t) + a_2 y_2(\Delta x_{12}(t)) + a_3 y_3(\Delta x_{12}(t)) \\ &= k_1 \Delta x_{12}(t) + a_2 \Delta x_{12}^2(t) + a_3 \Delta x_{12}^3(t). \end{aligned} \quad (31)$$

Estimates $\hat{H}_{11}^{[c2]}(\omega)$ and $\hat{H}_{11}^{[1]}(\omega)$ are illustrated in Figure 15(a). As shown, $\hat{H}_{11}^{[c2]}(\omega)$ closely matches true $H_{11}(\omega)$. Indication that D₁ is an accurate model is given by $\hat{\gamma}_{M1}^2(\omega)$ of Figure 15(b). Since both D₁ and A₁ are accurate, this illustrates that the identification process may not yield a unique model. The coherence function $\hat{\gamma}_{YF_1}^2(\omega)$ also shown in Figure 15(b) is similar to $\hat{\gamma}_{YF_1}^2(\omega)$ of Model A₁, Figure 6(b), suggesting that the two models are similar. The spectral means of $\hat{a}_2(\omega)$ and $\hat{a}_3(\omega)$ are $\langle \hat{a}_2(\omega) \rangle_\omega = 15.57 - 11.22i \text{ kN/m}^2$, $\langle \hat{a}_3(\omega) \rangle_\omega = 501.28 + 0.47i \text{ MN/m}^3$. The spectral mean $\langle \hat{a}_3(\omega) \rangle_\omega$ of the cubic non-linearity is an accurate estimate with an imaginary part three orders of magnitude less than the real part. However, the spectral mean $\langle \hat{a}_2(\omega) \rangle_\omega$ of the quadratic coefficient has an imaginary part of the same magnitude as the real part. This may serve as an indication that the quadratic term is not present in $f_{12}^e(t)$.

The cumulative study of Models A₁, B₁, C₁ and D₁ suggests a possible strategy one may employ for determining an accurate model for describing Example I. Although real systems may be more difficult to evaluate, coherence functions as illustrated here can provide significant clues and insight into the validity of models chosen and indicate the significance of each term included in the model $p_{12}^e(t)$ for actual $f_{12}^e(t)$. A final note concerning the presence of uncorrelated noise. As shown in this section, the cumulative coherence functions indicate when an inaccurate model is being employed by assuming values less than unity. And, as shown in section 5, the same is true when uncorrelated measurement noise is present in the excitation and response data. So, it is not possible to differentiate between the two errors when both are simultaneously present. Therefore, it is important to ensure, whenever possible, that measurement signals are noise free, or since this is not realistic, that noise levels are kept as low as possible.

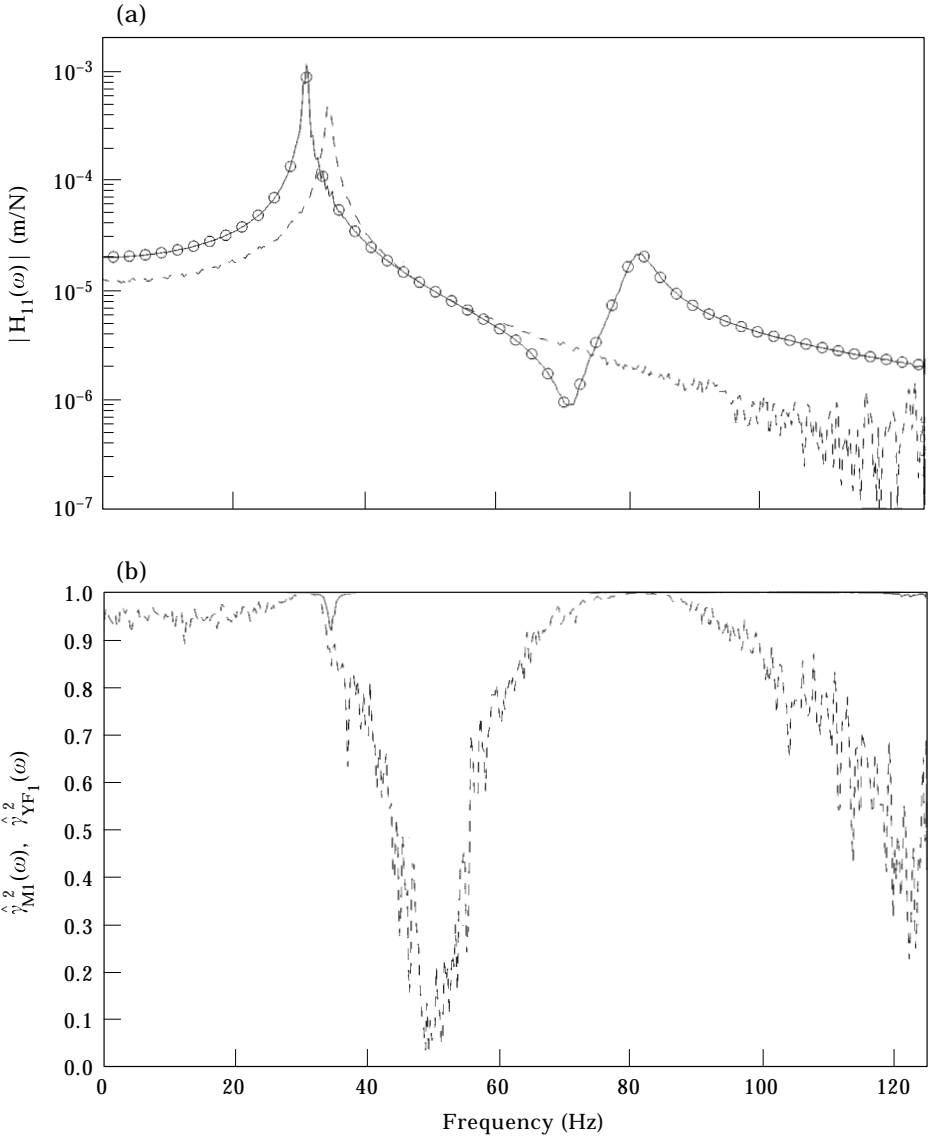


Figure 15. Spectra for Example I using Model D₁ for Spectral Method calculations. (a) Magnitude of $H_{11}(\omega)$. —, $\hat{H}_{11}^{e(2)}(\omega)$; ---, $\hat{H}_{11}^{(1)}(\omega)$; ○○○, $H_{11}(\omega)$. (b) Coherence functions $\hat{\gamma}_{M1}^2(\omega)$ and $\hat{\gamma}_{YF1}^2(\omega)$. —, $\hat{\gamma}_{M1}^2(\omega)$; ---, $\hat{\gamma}_{YF1}^2(\omega)$.

6.2. IDENTIFICATION OF EXAMPLE II

Models given in Table 6 are used next to identify Example II by the Spectral Method. Model A_{II} is composed of the correct terms to model $f_{12}^e(t)$; and, as listed in Table 7, the resulting estimates are accurate. Models B_{II} and C_{II} contain only a fifth order and only a quadratic term, respectively. These models were chosen to illustrate the consequences of leaving out a term from $p_{12}^e(t)$ to describe $f_{12}^e(t)$. As a result, neither model produces accurate estimates. However, comparison shows that inclusion of only the fifth order term, Model B_{II}, yields a better

estimate. Model D_{II} represents $f_{12}^e(t)$ by a cubic non-linearity. Modelling non-linearities by a cubic polynomial is a common assumption [12–15, 20]. However, as shown for this system, the model results in poor estimates. In fact, the estimated damping for the first mode is negative.

One possible strategy for modelling continuous non-linearities is by polynomial expansions. Models E_{II} and F_{II} represent $f_{12}^e(t)$ by expansions including linear through fifth order and linear through seventh order terms, respectively. As Table 7 shows, such models result in accurate estimates of the modal parameters. Notice that the spectral means of the coefficients of the quadratic $\langle \hat{a}_2(\omega) \rangle_\omega$ and fifth order $\langle \hat{a}_5(\omega) \rangle_\omega$ terms are well estimated with negligible imaginary parts, where as the other coefficients have spectral means with imaginary parts comparable to their real parts. This may serve as an indicator of which terms are truly present.

Models E_{II} and F_{II} both contain the correct terms of $f_{12}^e(t)$ which may be a reason why they result in accurate estimates. Therefore, the next models considered, G_{II}, H_{II} and I_{II}, which are polynomials of the seventh, ninth and twelfth order, respectively, explicitly exclude the correct terms. Although more error exists in the modal estimates using these models when compared with the modal estimates

TABLE 6
Models used in the estimation of Example II

Model	$p_{12}^e(t)$
A _{II}	$k_1 \Delta x_{12}(t) + a_2 y_2(\Delta x_{12}(t)) + a_5 y_3(\Delta x_{12}(t)) = k_1 \Delta x_{12}(t) + a_2 \Delta x_{12}^2(t) + a_5 \Delta x_{12}^5(t)$
B _{II}	$k_1 \Delta x_{12}(t) + a_5 y_5(\Delta x_{12}(t)) = k_1 \Delta x_{12}(t) + a_5 \Delta x_{12}^5(t)$
C _{II}	$k_1 \Delta x_{12}(t) + a_2 y_2(\Delta x_{12}(t)) = k_1 \Delta x_{12}(t) + a_2 \Delta x_{12}^2(t)$
D _{II}	$k_1 \Delta x_{12}(t) + a_3 y_3(\Delta x_{12}(t)) = k_1 \Delta x_{12}(t) + a_3 \Delta x_{12}^3(t)$
E _{II}	$k_1 \Delta x_{12}(t) + \sum_{j=2}^5 a_j y_j(\Delta x_{12}(t)) = k_1 \Delta x_{12}(t) + \sum_{j=2}^5 a_j \Delta x_{12}^j(t)$
F _{II}	$k_1 \Delta x_{12}(t) + \sum_{j=2}^7 a_j y_j(\Delta x_{12}(t)) = k_1 \Delta x_{12}(t) + \sum_{j=2}^7 a_j \Delta x_{12}^j(t)$
G _{II}	$k_1 \Delta x_{12}(t) + \sum_{\substack{j=3 \\ j \neq 5}}^7 a_j y_j(\Delta x_{12}(t)) = k_1 \Delta x_{12}(t) + \sum_{\substack{j=3 \\ j \neq 5}}^7 a_j \Delta x_{12}^j(t)$
H _{II}	$k_1 \Delta x_{12}(t) + \sum_{\substack{j=3 \\ j \neq 5}}^9 a_j y_j(\Delta x_{12}(t)) = k_1 \Delta x_{12}(t) + \sum_{\substack{j=3 \\ j \neq 5}}^9 a_j \Delta x_{12}^j(t)$
I _{II}	$k_1 \Delta x_{12}(t) + \sum_{\substack{j=3 \\ j \neq 5}}^{12} a_j y_j(\Delta x_{12}(t)) = k_1 \Delta x_{12}(t) + \sum_{\substack{j=3 \\ j \neq 5}}^{12} a_j \Delta x_{12}^j(t)$

TABLE 7
Estimated properties of Example II by the Spectral Method in the absence of noise

Model	Mode, <i>r</i>	$\hat{\omega}_r$ (Hz)	$\hat{\zeta}_r$ (%)	$\hat{\phi}_r$	Spectral mean of estimated coefficients of $y_r(t)$
A _{II}	1	31.0 (0.3)	1.0 (0.0)	{1.0, 0.6}	$\langle \hat{a}_2(\omega) \rangle_\omega = -1.0 - 8.6e-4i \text{ MN/m}^2$
	2	81.7 (0.4)	2.6 (0.0)	{-0.6, 1.0}	$\langle \hat{a}_5(\omega) \rangle_\omega = 10.0 - 9.1e-3i \text{ GN/m}^5$
B _{II}	1	30.6 (1.6)	0.6 (40.0)	{1.0, 0.6}	$\langle \hat{a}_5(\omega) \rangle_\omega = 5.7 - 0.2i \text{ GN/m}^5$
	2	87.4 (7.4)	2.0 (23.1)	{-0.5, 1.0}	
C _{II}	1	33.8 (8.7)	1.6 (60.0)	{1.0, 0.8}	$\langle \hat{a}_2(\omega) \rangle_\omega = -684.8 - 33.0i \text{ kN/m}^2$
	2	110.0 (35.1)	0.1 (96.2)	{-0.6 + 0.5i, 1.0}	
D _{II}	1	28.2 (9.3)	-0.1 (-)	{1.0, 0.6}	$\langle \hat{a}_5(\omega) \rangle_\omega = 22.1 - 2.2i \text{ MN/m}^3$
	2	85.5 (5.0)	1.2 (53.8)	{-0.3 + 0.1i, 1.0}	
E _{II}	1	31.1 (0.0)	0.9 (10.0)	{1.0, 0.6}	$\langle \hat{a}_2(\omega) \rangle_\omega = -1.0 + 3.3e-3i \text{ MN/m}^2$
	2	81.3 (0.1)	2.6 (0.0)	{-0.6, 1.0}	$\langle \hat{a}_3(\omega) \rangle_\omega = 494.8 - 114.5i \text{ kN/m}^3$ $\langle \hat{a}_4(\omega) \rangle_\omega = 257.4 - 773.4i \text{ kN/m}^4$ $\langle \hat{a}_5(\omega) \rangle_\omega = 9.9 - 6.3e-3i \text{ GN/m}^5$
F _{II}	1	31.0 (0.3)	0.3 (70.0)	{1.0, 0.6}	$\langle \hat{a}_2(\omega) \rangle_\omega = -1.0 + 2.4e-3i \text{ MN/m}^2$
	2	81.3 (0.1)	2.6 (0.0)	{-0.6, 1.0}	$\langle \hat{a}_3(\omega) \rangle_\omega = 1.4 - 0.1i \text{ MN/m}^3$ $\langle \hat{a}_4(\omega) \rangle_\omega = 3.0 - 0.2i \text{ MN/m}^4$ $\langle \hat{a}_5(\omega) \rangle_\omega = 10.0 - 8.0e-3i \text{ GN/m}^5$ $\langle \hat{a}_6(\omega) \rangle_\omega = -422.6 - 229.5i \text{ MN/m}^6$ $\langle \hat{a}_7(\omega) \rangle_\omega = 31.5 - 0.2i \text{ GN/m}^7$

G _{II}	1	30.0 (3.5)	0.2 (80.0)	{1.0, 0.6}	$\langle \hat{a}_3(\omega) \rangle_\omega = 26.1 - 0.9i \text{ MN/m}^3$ $\langle \hat{a}_4(\omega) \rangle_\omega = -466.5 + 9.7i \text{ MN/m}^4$ $\langle \hat{a}_6(\omega) \rangle_\omega = 53.9 - 2.2i \text{ GN/m}^6$ $\langle \hat{a}_7(\omega) \rangle_\omega = 976.8 + 3.0i \text{ GN/m}^7$
	2	77.0 (5.4)	1.7 (34.6)	{-0.5, 1.0}	
H _{II}	1	30.6 (1.6)	0.5 (50.0)	{1.0, 0.6}	$\langle \hat{a}_3(\omega) \rangle_\omega = 19.2 - 0.4i \text{ MN/m}^3$ $\langle \hat{a}_4(\omega) \rangle_\omega = -819.8 + 7.7i \text{ MN/m}^4$ $\langle \hat{a}_6(\omega) \rangle_\omega = 216.8 - 3.8i \text{ GN/m}^6$ $\langle \hat{a}_7(\omega) \rangle_\omega = 1815.4 + 22.9i \text{ GN/m}^7$ $\langle \hat{a}_8(\omega) \rangle_\omega = -17.8 + 0.4i \text{ TN/m}^8$ $\langle \hat{a}_9(\omega) \rangle_\omega = -102.2 - 4.1i \text{ TN/m}^9$
	2	78.6 (3.4)	2.0 (30.0)	{-0.6, 1.0}	
I _{II}	1	30.6 (1.6)	0.5 (50.0)	{1.6, 1.0}	$\langle \hat{a}_3(\omega) \rangle_\omega = 12.2 + 1.6e-2i \text{ MN/m}^3$ $\langle \hat{a}_4(\omega) \rangle_\omega = -1.6 + 3.4e-2i \text{ GN/m}^4$ $\langle \hat{a}_6(\omega) \rangle_\omega = 980.5 - 42.4i \text{ GN/m}^6$ $\langle \hat{a}_7(\omega) \rangle_\omega = 3.5 - 6.8e-2i \text{ TN/m}^7$ $\langle \hat{a}_8(\omega) \rangle_\omega = -269.1 + 17.5i \text{ TN/m}^8$ $\langle \hat{a}_9(\omega) \rangle_\omega = -526.3 + 25.8i \text{ TN/m}^9$ $\langle \hat{a}_{10}(\omega) \rangle_\omega = 34.0 - 3.0i \text{ PN/m}^{10}$ $\langle \hat{a}_{11}(\omega) \rangle_\omega = 28.7 - 2.5i \text{ PN/m}^{11}$ $\langle \hat{a}_{12}(\omega) \rangle_\omega = -1.6 + 0.8i \text{ EN/m}^{12}$
	2	80.4 (1.2)	2.5 (3.8)	{1.0, -1.6}	

% Error = (|estimated - true|/true) · 100, given in parentheses.

using Models E_{II} and F_{II}, the error tends to decrease with increasing terms. This suggests that polynomial expansions may be successful for estimating non-linearities. It should however be noted, that an increase in the number of terms in the polynomial expansion also increases the computation of the conditioned spectral density matrices necessary for the Spectral Method. The same is true of the Temporal Method since the increased computation entails the inversion of an increasingly larger system matrix. Also, note that the use of higher order polynomial expansions may not lead to one unique model since many models including A_{II}, E_{II}, F_{II}, G_{II}, H_{II} and I_{II} produce relatively accurate results.

7. NON-LINEARITY WITH NON-INTEGER EXPONENT

The final example is considered to examine the difficulties of identifying a system with a non-polynomial but continuous type non-linearity. This system maintains the identical linear parameters of Examples I and II, however, $f_{12}^e(t)$ now contains a term with a non-integer exponent, similar to non-linearities caused by Hertzian contact forces [21]. This is designated as Example IV,

$$f_{12}^e(t) = k_1 \Delta x_{12}(t) + \eta \cdot \text{sgn}(\Delta x_{12}(t)) |\Delta x_{12}(t)|^{1.8}, \quad \eta = 1.0 \text{ MN/m}^{1.8}, \quad (32a, b)$$

where $\text{sgn}(\Delta x_{12}(t)) = \Delta x_{12}(t)/|\Delta x_{12}(t)|$. First, to illustrate that this type of system can in fact be identified given the correct non-linear mathematical form, Model A_{IV} is employed that assumes the true form as

$$\begin{aligned} \text{Model A}_{IV}: \quad p_{12}^e(t) &= k_1 x_{12}(t) + a \cdot y(t) = k_1 \Delta x_{12}(t) \\ &+ a \cdot \text{sgn}(\Delta x_{12}(t)) |\Delta x_{12}(t)|^{1.8}. \end{aligned} \quad (33)$$

As shown in Figure 16(a), $\hat{H}_{11}^{[e2]}(\omega)$ accurately estimates the true $H_{11}(\omega)$. However, in practice, as with the other examples, the *a priori* knowledge of the mathematical form of $f_{12}^e(t)$ may be unknown. Therefore, as executed with Example II, a more plausible strategy is to estimate (32a) with a polynomial expansion given by

$$\begin{aligned} \text{Model B}_{IV}: \quad p_{12}^e(t) &= k_1 \Delta x_{12}(t) + \sum_{i=2}^n a_i y_i(\Delta x_{12}(t)) \\ &= k_1 \Delta x_{12}(t) + \sum_{i=2}^n a_i \Delta x_{12}^i(t). \end{aligned} \quad (34)$$

Model B_{IV} is applied to Example IV for values of $n = 5$ and 10 . Resulting $\hat{H}_{11}^{[e2]}(\omega)$ are shown in Figure 16(b). Note that $n = 10$ is the largest possible value that could be chosen without numerical conditioning problems to arise. As can be seen from Figure 16(b), $\hat{H}_{11}^{[e2]}(\omega)$ improves with increasing values of n . This increase in accuracy is also indicated by $\hat{\gamma}_{M1}^2(\omega)$ of Figure 17(a). Notice the y -axis is displayed only from 0.88 to unity in order to illustrate the differences between the two curves. Shown in Figure 17(b) are estimated stiffness curves for $n = 5$ and 10 along with the true stiffness curve. Note, however, the Spectral Method estimates linear modal parameters and not physical parameters such as k_1 . Hence, these curves do not

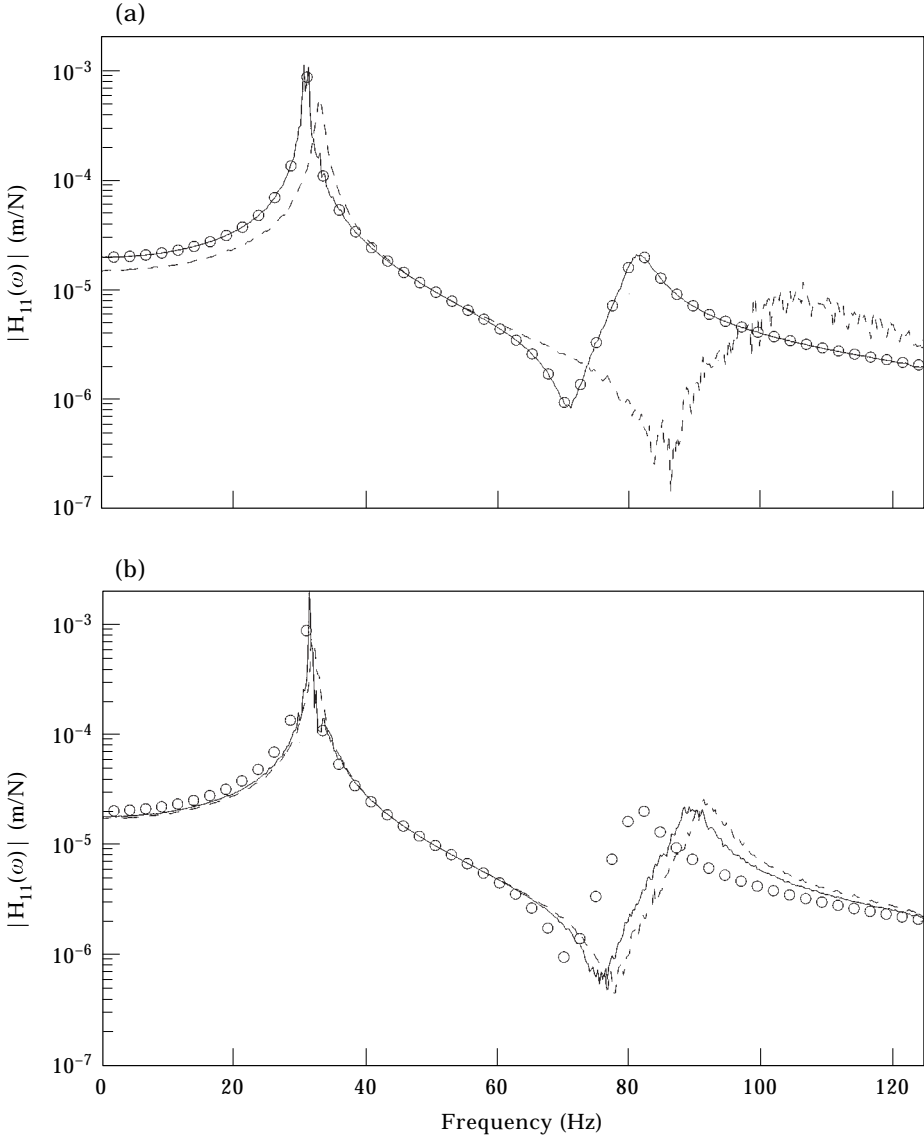


Figure 16. Magnitude of Dynamic compliance functions of Example IV. (a) Model A_{IV} used for “ H_{c2} ” estimate. —, $\hat{H}_{11}^{(c2)}(\omega)$; ---, $\hat{H}_{11}^{(1)}(\omega)$; ○○○, $H_{21}(\omega)$. (b) Model B_{IV} used for “ H_{c2} ” estimate. —, $\hat{H}_{11}^{(c2)}(\omega)$ with $n=10$; ---, $\hat{H}_{11}^{(c2)}(\omega)$ with $n=5$; ○○○, $H_{21}(\omega)$.

include the linear stiffness term and accordingly one should not interpret these plots as physical stiffness curves. As shown, the estimated non-linear stiffness approaches the true with increasing n . This example suggests that the employment of polynomial expansions to describe the unknown non-linearities may be a successful strategy once numerical conditioning errors are eliminated so that additional terms can be included in the model. Further examination of non-integer exponent type non-linearities as given by equation (32a) is needed since literature on this subject is sparse.

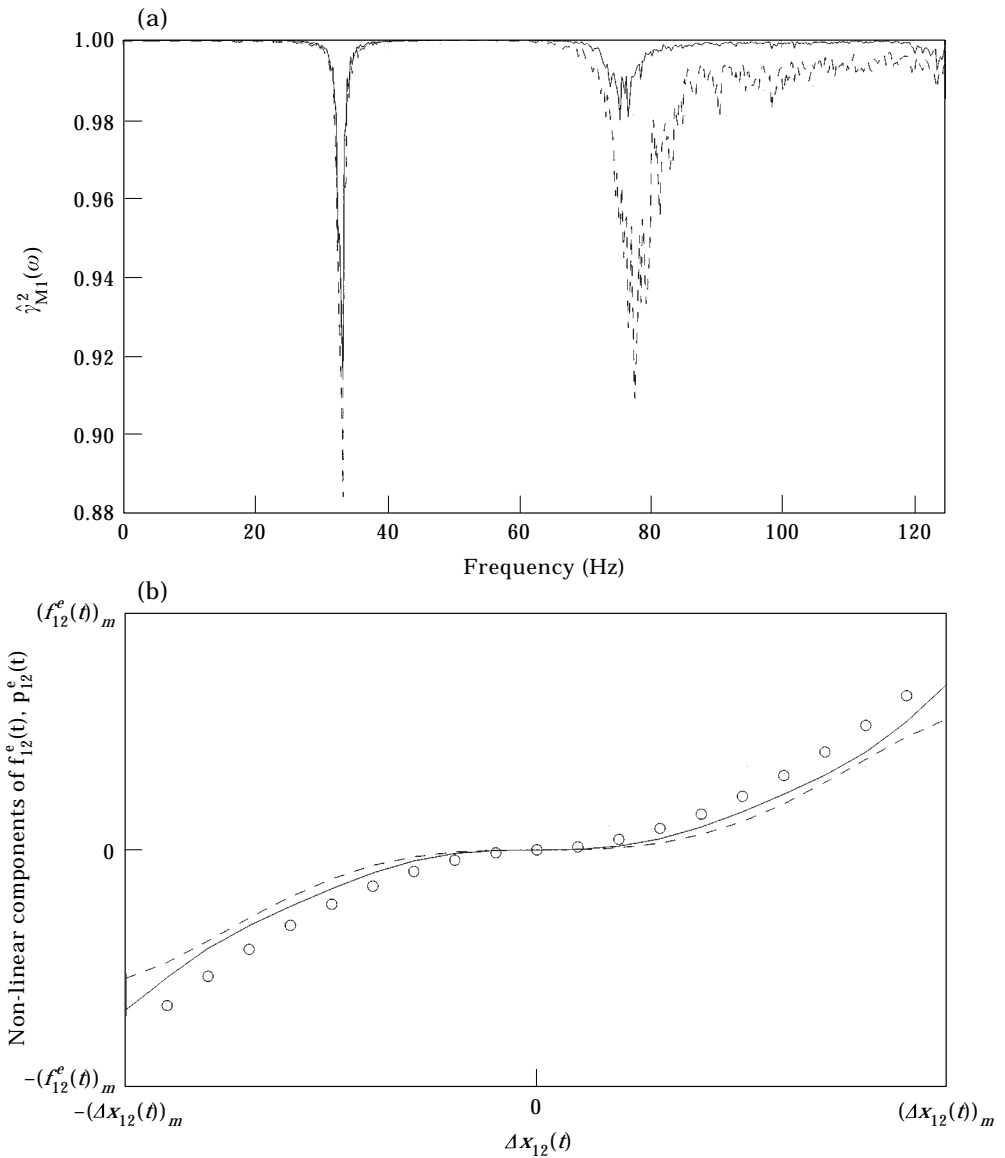


Figure 17. Cumulative coherence and stiffness estimates of Example IV. (a) Cumulative coherence of Model B_{IV}. —, $\hat{\gamma}_{MI}^2(\omega)$ with $n=10$; ---, $\hat{\gamma}_{MI}^2(\omega)$ with $n=5$. (b) Non-linear components of stiffness estimates. —, $\hat{p}_{i_2}^e(t)$ with $n=10$; ---, $\hat{p}_{i_2}^e(t)$ with $n=5$; ○○○, $f_{i_2}^e(t)$.

8. CONCLUSION

When identifying non-linear mechanical and structural systems, some *a priori* knowledge of the nature and mathematical form of the non-linearities is necessary. Nonetheless, a unique model is still not guaranteed since this knowledge may be limited and different mathematical formulae for describing the non-linearities may result in reasonably accurate estimates. Also, the presence of uncorrelated noise often corrupts the response and excitation data. These problems have been

illustrated here by four simulation systems, and for two of these examples, in the presence of moderate and high measurement noise levels. Both the Restoring Force Temporal Method [10, 11] and the “Reverse Path” Spectral Method [7] have been employed for identification. Although each technique has its own merits, this article does not attempt to quantifiably compare their performance but rather illustrates that the problems addressed here are not method dependent; instead they must be addressed regardless of whichever technique is employed. Coherence functions have been developed based on the Spectral Method and their application has been demonstrated. These coherence functions indicate the level of uncorrelated noise present in the data and also indicate when reasonably accurate models have been chosen to describe the non-linear systems. Therefore, parameters estimated by techniques such as the ones discussed here can be assessed with some level of confidence.

With the capability of now being able to indicate the accuracy of the mathematical models chosen to describe non-linear systems, ongoing and future research will extend the identification techniques examined here to other complex problems including damping non-linearities. The next promising area appears to be the non-integer non-linearity which has sparsely been addressed in the scientific literature [21]. Future research will also focus on enhancing conditioned and unconditioned spectral density functions that are corrupted by uncorrelated measurement noise. A reference method [19] will act as a starting point for such an investigation. Also, time domain averaging operations and cross-correlation techniques may be adapted to improve the Restoring Force Method in the presence of uncorrelated measurement noise.

ACKNOWLEDGMENT

The authors wish to acknowledge the U.S. Army Research Office (URI Grant DAAL-03-92-G-0120 and the ASSERT Project; Project Monitor: Dr T. L. Doligalski) and the Chrysler Challenge Fund (Project Monitor: T. McCarthy) for supporting this study.

REFERENCES

1. R. J. ALLEMANG and D. L. BROWN 1998 *Journal of Sound and Vibration* **211**, 301–322. A unified matrix polynomial approach to modal identification.
2. L. D. MITCHELL 1982 *American Society of Mechanical Engineers, Journal of Mechanical Design* **104**, 277–279. Improved methods for the Fast Fourier Transform (FFT) calculation of the frequency response function.
3. H. K. MILNE 1984 *Journal of Sound and Vibration* **93**, 469–471. A note on the calculation of frequency response functions by the inverse method.
4. M. FRENCH JANUARY 1998 *Sound & Vibration*, 26–30. Contact problems in modal analysis.
5. H. R. BUSBY, C. NOPPORN and R. SINGH 1986 *Journal of Sound and Vibration* **180**, 415–427. Experimental modal analysis of non-linear systems: a feasibility study.
6. J. S. BENDAT and A. G. PIERSOL 1980 *Engineering Applications of Correlation and Spectral Analysis*. New York: Wiley-Interscience.

7. C. M. RICHARDS and R. SINGH 1998 *Journal of Sound and Vibration* **213**, 673–708. Identification of multi-degree-of-freedom nonlinear systems under random excitations by the “reverse path” spectral method.
8. S. F. MASRI and T. K. CAUGHEY 1979 *ASME, Journal of Applied Mechanics* **46**, 433–447. A nonparametric identification technique for nonlinear dynamic problems.
9. S. F. MASRI, H. SASSI and T. K. CAUGHEY 1982 *ASME, Journal of Applied Mechanics* **49**, 619–628. Nonparametric identification of nearly arbitrary nonlinear systems.
10. K. S. MOHAMMAD, K. WORDEN and G. R. TOMLINSON 1992 *Journal of Sound and Vibration* **152**, 471–499. Direct parameter estimation for linear and non-linear structures.
11. Y. YANG and S. R. IBRAHIM 1985 *Journal of Vibration, Acoustics, Stress, and Reliability in Design* **107**, 60–66. A nonparametric identification technique for a variety of discrete nonlinear vibrating systems.
12. J. S. BENDAT 1990 *Nonlinear System Analysis and Identification from Random Data*. New York: Wiley.
13. J. S. BENDAT, P. A. PALO and R. N. COPPOLINO 1992 *Probabilistic Engineering Mechanics*, 43–61. A general identification technique for nonlinear differential equations of motion.
14. J. S. BENDAT 1993 *Shock and Vibration* **1**, 21–31. Spectral techniques for nonlinear system analysis and identification.
15. J. S. BENDAT, R. N. COPPOLINO and P. A. PALO 1995 *International Journal of Non-Linear Mechanics* **30**, 841–860. Identification of physical parameters with memory in non-linear systems.
16. J. S. BENDAT and A. G. PIERSOL 1986 *Random Data: Analysis and Measurement Procedures*. New York: Wiley-Interscience; second edition.
17. G. KIM and R. SINGH 1995 *Journal of Sound and Vibration* **179**, 427–453. A study of passive and adaptive hydraulic engine mount systems with emphasis on non-linear characteristics.
18. GENRAD, INC. 1994 *The Star System Reference Guide*.
19. G. C. STEYER and R. SINGH 1987 *Journal of the Acoustical Society of America* **81**, 1955–1961. Alternative spectral formulations for acoustic velocity measurement.
20. T. J. ROYSTON and R. SINGH 1996 *Journal of Sound and Vibration* **198**, 279–298. Experimental study of a mechanical system containing a local continuous stiffness non-linearity under periodic excitations and a static load.
21. T. C. LIM and R. SINGH 1990 *Journal of Sound and Vibration* **139**, 179–199. Vibration transmission through rolling element bearings, part I: bearing stiffness formulation.

APPENDIX A: LIST OF SYMBOLS

a	coefficient vector of nonlinear functions
<i>a</i>	coefficient non-linear functions
B (ω)	linear dynamic stiffness matrix
<i>c</i>	linear damping coefficient
C	linear damping matrix
d ($\mathbf{x}(t)$, $\dot{\mathbf{x}}(t)$)	vector of motion dependent restoring force functions
$f_{12}^e(t)$	elastic force acting on m_1
f (t)	generalized excitation vector with Gaussian time history
F (ω)	spectra of f (t)
G (ω)	single-sided cross-spectral density matrix
H (ω)	linear dynamic compliance matrix
<i>i</i>	$\sqrt{-1}$
<i>k</i>	linear stiffness element
K	linear stiffness matrix
L (ω)	frequency response function between non-linear function Y (ω) and F (ω)

m	mass
\mathbf{M}	mass matrix
n	number of types of non-linearities
$\mathbf{n}(t)$	uncorrelated noise vector
N	dimension of system
$\mathbf{N}(\omega)$	vector of uncorrelated noise spectra
$p_{12}^e(t)$	assumed model of $f_{12}^e(t)$
t	time
T	time window
$\mathbf{x}(t)$	generalized displacement vector
$\mathbf{X}(\omega)$	spectra of $\mathbf{x}(t)$
$y(\Delta x_{12}(t))$	non-linear function
$Y(\omega)$	spectra of $y(\Delta x_{12}(t))$
$\mathbf{z}(\mathbf{x}(t), \dot{\mathbf{x}}(t))$	vector of the assumed form of the system's constraint forces
β	coefficient of polynomial term describing $f_{12}^e(t)$ for Examples I–III
ϕ	mode shape
Δt	time step for numerical simulation
$\Delta x_{12}(t)$	relative displacement = $x_1(t) - x_2(t)$
$\hat{\gamma}^2(\omega)$	ordinary coherence function
$\Gamma(\omega)$	Fourier transform of $\mathbf{d}(\mathbf{x}(t), \dot{\mathbf{x}}(t))$
η	coefficient of polynomial term describing $f_{12}^e(t)$ for Example IV
ω	frequency or natural frequency
$\hat{\xi}^2(\omega)$	partial coherence function
ζ	damping ratio
$\{0\}, \mathbf{0}$	null vector and matrix

Operators

$E[\cdot]$	expected value
$F[\cdot]$	Fourier transform
$\text{Im}[\cdot]$	imaginary part
$\text{Re}[\cdot]$	real part
$\langle \cdot \rangle_\omega$	spectral mean

Subscripts

$c1, c2$	conditioned estimates of \mathbf{H}
e	effective matrix determined from linearization
F	excitation vector
i	i th mass location
j	j th non-linear function
$(+j)$	correlated with the j th non-linear function
$(-1:j)$	uncorrelated with the 1st through the j th non-linear function
$(-1:n)$	uncorrelated with the 1st through the n th non-linear function, i.e., linear component
M	signifies cumulative coherence function
n	contains only non-linear restoring force terms
N	uncorrelated noise
r	r th mode
X	response vector
Y	coherence function which indicates contribution from non-linearities

Superscripts

*	complex conjugate
T	transpose
-1	inverse
[1]	" H_1 " estimate
[c1]	" H_{c1} " estimate
[c2]	" H_{c2} " estimate

Embellishments

~	quantity contaminated by noise
^	estimated quantity
·	first derivative with respect to time
··	second derivative with respect to time